Construction Robotics (2024) 8:20
https://doi.org/10.1007/s41693-024-00137-7

ORIGINAL PAPER

Scaffold-free cooperative robotic disassembly and reuse of a timber structure in the ZeroWaste project

Edvard P. G. Bruun[1] · Erin Besler[2] · Sigrid Adriaenssens[3] · Stefana Parascho[4]

Received: 18 March 2024 / Accepted: 22 July 2024 / Published online: 18 August 2024

Abstract

ZeroWaste as a project aims to reposition existing timber building stock within a circular economy framework, reframing them as valuable resources for reuse rather than disposal. This paper presents the computational methods and physical construction outcomes of the project, showcasing how the circular economy principles of reuse and reduced material consumption can be actualized through cooperative robotic fabrication. Initially, a pavilion-scale prototype, mirroring conventional North American stick frame construction, is constructed. A robotic cell, equipped with three large-scale robotic arms and 3D cameras, is used to generate precise as-built geometric data on the prototype, which is used for planning robotic processes. A novel topological representation of a structure, the support hierarchy graph, is developed and used to generate candidate fabrication sequences. These sequences are then assessed for robotic execution and structural feasibility. Leveraging the cooperative nature of the setup, these sequences are planned without requiring external scaffolding for structural stability as the robots are used to provide temporary support during the fabrication process. Three physical case studies validate the developed computational and cooperative robotic workflow. In Phase 1 we perform a small-scale disassembly intervention by planning the removal of a single member. In Phase 2 we expand the disassembly scope to the full South wall and perform a minor reassembly at the end of the disassembly sequence. In Phase 3 we expand the scope further, disassembling all remaining members in the West wall and roof sub-structures while performing a concurrent one-to-one reassembly process, where each member removed is placed back into the structure to turn the typical stud wall into a stiffer lattice structure. The successful completion of the three case studies demonstrates the potential for existing buildings to serve as reservoirs of reusable materials through scaffold-free cooperative robotic disassembly and reassembly.

Keywords Circular economy · Timber · Disassembly · Reuse · Cooperative · Robot · Scaffold-free

1 Introduction

The Architecture, Engineering, Construction (AEC) industry has a significant negative impact on the environment due to its material and energy-intensive manufacturing and construction processes (International Energy Agency 2018) and the high embodied carbon content of structural systems (Kaethner and Burridge 2012; Fang et al. 2023). For example, buildings and construction activities accounted for 36% of global energy-usage and of 37% of global CO2 emissions in 2020 (United Nations 2021). This impact is further exacerbated by the increasing waste generated by construction and demolition (C&D) processes (US EPA 2018, 2020b), which were estimated to account for up to 30% of total waste produced globally in the 1990s (Purchase et al. 2022; Fishbein 1998).

✉ Edvard P. G. Bruun
edvard.bruun@gatech.edu

Erin Besler
ebesler@princeton.edu

Sigrid Adriaenssens
sadriaen@princeton.edu

Stefana Parascho
stefana.parascho@epfl.ch

[1] School of Civil and Environmental Engineering, Georgia Institute of Technology, Atlanta, USA

[2] School of Architecture, Princeton University, Princeton, USA

[3] Civil and Environmental Engineering, Princeton University, Princeton, NJ, USA

[4] School of Architecture, Civil and Environmental Engineering, Swiss Federal Institute of Technology, Lausanne, Switzerland

To illustrate this worsening trend, in the mid-1990s in the United States, construction and demolition (C&D) activities were responsible for generating an estimated 100–135 million tons of waste, of which approximately 35–45% found its way to landfills (Mills et al. 1999; US EPA 1998). This C&D waste accounted for 29% of the total landfill volumes at that time (Lu and Yuan 2011). However, by 2018, the volume of waste from C&D activities had surged to 600 million tons, with 144 million tons or 24% of this waste ending up in landfills (US EPA 2020a). Thus, approximately half of landfill volumes in 2018 were associated with C&D activities, with the remaining municipal solid waste contributing 146 million tons (US EPA 2020a). This trend is especially concerning when considering the substantial construction needs of the coming century. Aging infrastructure must be replaced while accommodating the requirements of a growing and rapidly urbanizing global population (Ritchie et al. 2024).

When looking at C&D activities specifically, demolition accounts for approximately 90% of debris generation while construction activities only account for 10% (US EPA 2020a). This statistic underscores the urgent need for transformation within the industry with respect to demolition. Therefore, exploring novel approaches that emphasize deconstruction and material reuse, aligning with the principles of a circular economy (Geissdoerfer et al. 2017), presents a promising solution to the industry's waste challenges. Research indicates that a significant portion of construction waste originates from inadequate waste reduction measures at the beginning of a building's life-cycle, in early in the design stages, particularly in planning for building decommissioning (Osmani et al. 2008). In this paper, we address the challenges that also exist at the other end of the building life-cycle. We leverage technological advancements such as robotics and automation to assist in the decommissioning process, thus addressing the waste generated at the end of an existing structure's life.

1.1 Paper organization

The paper begins with Sect. 2, where we present a literature review, covering topics such as circular economy design frameworks, robots in the construction industry, and cooperative robotic fabrication specifically within the context of material circularity. We also provide an overview of the ZeroWaste project on which this paper is based, describing how the project addresses circular economy and robotic fabrication through its research objectives. Following this, in Sect. 3, we outline the experimental setup, describing the physical robotic fabrication cell and the experimental prototype that is built and then experimented on in the three subsequent project phases. In Sect. 4, we detail the workflow and methods, focusing on the computational methods developed for various aspects of the project. This includes the use of robot-mounted 3D cameras to gather geometric information about the as-built conditions of the structure, the development of the topological support hierarchy representation, and the methods used to generate robotic fabrication sequences and assess their feasibility. In Sect. 5, we present and discuss the results of implementing the computational methods described in the previous section to plan and then execute three different disassembly and reassembly robotic fabrication case studies on the prototype structure. Finally, in Sect. 6, we conclude the paper, summarizing the main results and discussions from the case studies performed on the prototype structure, and suggesting ideas for future work stemming from the limitations of the current work.

2 Literature review

2.1 Circular economy design frameworks

The construction industry is actively moving away from the traditional linear single-use material flow model. To support this transition, there has been a focus on developing models for quantifying the environmental benefits of material circularity and the potential for reusing existing building stock (Cottafava and Ritzen 2021; Eberhardt et al. 2021). In parallel, novel frameworks have emerged that break down the concept of circularity into distinct principles relating to material and energy flows. An illustrative framework is the "narrow, slow, close, and regenerate" framework outlined in Konietzko et al. (2020), Çetin et al. (2021), which also serves as the foundation for a recent book on shifting to the circular built environment while leveraging modern digital technologies (De Wolf et al. 2023).

The "slow" principle, which focuses on extending the lifespan of products and components, encompasses a range of circular product design and business strategies that are applicable to the building industry (Bocken et al. 2016). One such strategy, known as "design for dis- and reassembly," is demonstrated by a growing body of research that highlights the practical implementation of design and optimization strategies for the disassembly, reuse, and reconfiguration of discrete element structures such as planar trusses, space frames, moment frames, and reciprocal frames. Due to the diverse range of structural types and material systems, a variety of disassembly approaches exist, leveraging principles such as reversible and interlocking connections (Naboni et al. 2021; Glath et al. 2022; Zahiri 2023), designing reusable joints that can be used for different structural configurations (Brütting et al. 2021), planning for reuse through a kit of parts optimization (Brütting et al. 2019, 2020), or using rigidity theory to design structures that can be taken apart efficiently in a modular way (Bruun et al. 2022a).

These projects, emphasizing the "slow" principle by addressing the design stage for a structure, are a definite inspiration for the current project. But the focus of the project described in this paper is more directly aligned with aspects of the "narrow" principle, aimed at reducing the primary resource inputs into construction activities associated with disassembly, as well as the "close" principle, aimed at demonstrating applications of reuse and reassembly for existing structures.

2.2 Robots in the construction industry

The construction industry has been slower in adopting automation technology compared to other sectors, despite its potential for efficiency gains (Barbosa et al. 2017). Nonetheless, there remains an opportunity to harness modern technological innovations, particularly in the utilization of robots, to enhance construction productivity (The Business Research Company 2023). This is particularly relevant in the construction of intricate and efficient customized structures, where robots can excel in precise repetitive movements, accurate spatial positioning, and sustained task performance (García de Soto et al. 2018).

In the 1980s, the initial phase of integrating robots into construction focused on automating individual tasks using a single robots (Bock 2007; Bock and Linner 2016). However, recent years have witnessed a shift towards incorporating robots into broader contexts, employing more complex robotic setups for collaborative and adaptive construction processes (Parascho 2023). Over the last two decades, digital fabrication (dfab) has garnered attention in both the construction industry and academia, aiming to expand geometric design possibilities through robot utilization (Gramazio and Kohler 2008, 2014). Departing from task-specific applications, dfab demonstrates how robotic fabrication can be used for more general-purpose tasks in creating complex and customized structures.

The dfab movement first saw robots employed in constructing prefabricated load-bearing walls with non-standardized profiles using discrete volumetric elements (Bonwetsch et al. 2006, 2007; Kohler et al. 2014). However, these robotic applications to discrete element brick structures primarily focused on vertical layer-based construction (Bärtschi et al. 2010; Piškorec et al. 2018; Dörfler et al. 2016; Gifthaler et al. 2017). Subsequent projects, such as the DFAB house, demonstrated how digital design and robotic fabrication processes could produce diverse non-standardized components for assembly into a building-scale structure (Willmann et al. 2016; Hack et al. 2017, 2020). Other dfab examples illustrate the breadth of applications possible when utilizing robots, including cutting doubly-curved surfaces for custom formwork out of foam blocks (Søndergaard et al. 2016), constructing timber wall modules from non-standardized members (Thoma et al. 2018), winding fibers to create modular panels for shell structures (Doerstelmann et al. 2015), and building branching structures using foam blocks (Wu and Kilian 2018).

2.3 Cooperative robotics and material circularity

Cooperative robotic fabrication, a specialized form of robotic manufacturing, entails synchronized robotic agents working together to achieve greater system utility and unique outcomes that would be unattainable with independent robot operation (Cao et al. 1997). In this paper, we distinguish a cooperative robotic process from a collaborative robotic process, where the later refers to processes where human operators perform complementary actions alongside robotic setups (i.e., human-robot collaboration) (Amtsberg et al. 2021; Yang et al. 2024). Yet cooperative and collaborative processes are not mutually exclusive, as collaboration between humans and a multi-robot setup can occur while robotic agents are either working cooperatively (Bruun et al. 2020) or non-cooperatively (Weckenborg et al. 2020; Shi et al. 2012).

The use of a cooperative robotic fabrication approach as a subset the dfab research domain, for construction at the building-scale, was first demonstrated in Parascho et al. (2017), Parascho et al. (2018). Cooperative robotic fabrication since has emerged as a promising approach, showing the potential to enhance fabrication complexity and the degree to which a process can be automated (Bruun et al. 2021; Mesnil et al. 2023). However, the utilization of multiple robots working together offers additional benefits. A review summarizing examples of cooperative robotic fabrication across the construction industry, focusing on how it addresses principles of circular economy and material circularity, illustrates this point (Bruun et al. 2024). This review highlights several projects demonstrating material reuse and reduction by achieving scaffold-free assembly and disassembly. The cooperative function of the robotic setup (i.e., support/place/remove sequencing) used for the project described in this paper, is directly inspired by the previous applications summarized in this review. For example, multiple robotic arms were cooperatively sequenced to support the central arch of a masonry vault during its assembly (Parascho et al. 2020, 2021; Han et al. 2020), and were used to stabilize a timber space frame arch structure during its assembly and disassembly (Bruun et al. 2022a).

2.4 The ZeroWaste project

This paper presents the results of the ZeroWaste project, which serves as a practical demonstrator and a pivotal link between design frameworks based on material circularity (Sect. 2.1) and the use of robotic automation technology

in the construction industry (Sects. 2.2 and 2.3). While our project bears the title "ZeroWaste," we acknowledge that its literal interpretation may be misleading. We wish to clarify that our aim is to set forth an aspirational objective for the robotic workflow and methods explored within the "close" and "narrow" principles of a circular economy. We do not claim that our project eliminates waste entirely or has zero environmental impact.

Our research is conducted on a prefabricated timber prototype, which is meant to represent a generic unknown existing structure built according to the common North American stick frame construction practices. This choice is based on the prevalence of this building type coupled with the frequency that timber buildings are disposed of at the end of their lives, as noted in previous studies (O'Brien et al. 2006; Diyamandoglu and Fortuna 2015). Notably, of the 40.8 million tons of wood construction debris generated in 2018 in the US, 72% of this total is sent to landfills, where 92% of this amount is attributed to demolition processes (US EPA 2020a). To address this linear material flow, we propose reimagining timber buildings as material depots, recognizing their potential as reservoirs of valuable resources in the context of a circular economy (Zimmann et al. 2016). This shift prioritizes the upstream flow of materials on construction sites, reducing reliance on upstream virgin materials and downstream recycling and waste industries (Garcia et al. 2021). In addition, we aim to perform all processes in a scaffold-free manner to reduce the materials typically required to provide support during assembly and disassembly.

2.4.1 Research objectives

The ZeroWaste project is situated at the intersection of two key research areas: (1) circular economy and (2) robotic fabrication. The project aims to achieve various objectives that highlight the possibilities and benefits of combining these two research domains.

The objectives related to circular economy principles are the following:

1. *Physical Case Study:* Demonstrate how existing timber buildings can serve as reservoirs of reusable materials.
2. *Material Reduction (narrow principle)*: Avoid the use of external temporary supporting structures during construction.
3. *Material Reuse (close principle):* Build new structural configurations from reused material.

The objectives related to robotic fabrication are the following:

1. *Cooperative Fabrication:* Harness the capabilities of a three-robot robotic setup working in a coordinated manner.
2. *Fabrication Sequences:* Calculate feasible disassembly and reassembly sequences when considering constraints related to robotic reachability and structural stability.
3. *Scaffold-free Construction:* Execute the disassembly and reassembly sequences in a safe and controlled manner without the need for external temporary scaffolding, utilizing the robots themselves as passive structural supports.

The significance of these objectives extends beyond the specific structural prototype under study. They offer a versatile framework applicable to a wide range of timber structures and discrete element structural types. The ZeroWaste project serves as an illustration of how circular economy principles can be integrated into construction practices, and it highlights the potential for modern robotic fabrication setups to streamline the complex processes involved in efficient disassembly and reuse of building components.

2.4.2 Relationship to previous work

The current paper expands upon the initial findings documented in a work-in-progress paper presented at the 42nd Annual Conference of the Association for Computer Aided Design in Architecture (ACADIA) and published in the subsequent proceedings (Bruun et al. 2022b). The earlier paper focused solely on the preliminary stages of the project, providing an overview of the computational methods and their planned application to Phase 1. However, it did not include any physical implementation results. The current paper presents a comprehensive explanation of all the computational methods that were developed, as well as detailed planning, execution, and results for all three project phases. References to the original work are provided where images are adapted or reused in this paper.

3 Experimental setup

3.1 Robotic fabrication cell

The cooperative robotic cell employed in this study is illustrated schematically in Fig. 1. It features two IRB4600-40/2.55 robotic arms mounted on parallel linear tracks, providing a maximum travel distance of 3.9 m in the North–South direction. Positioned at the South end of the cell is an IRB7600-400/2.55 robotic arm securely fixed to the ground. All three robots are equipped with standard linear grippers featuring custom fingers tailored for pick-and-place operations involving dimensional lumber.

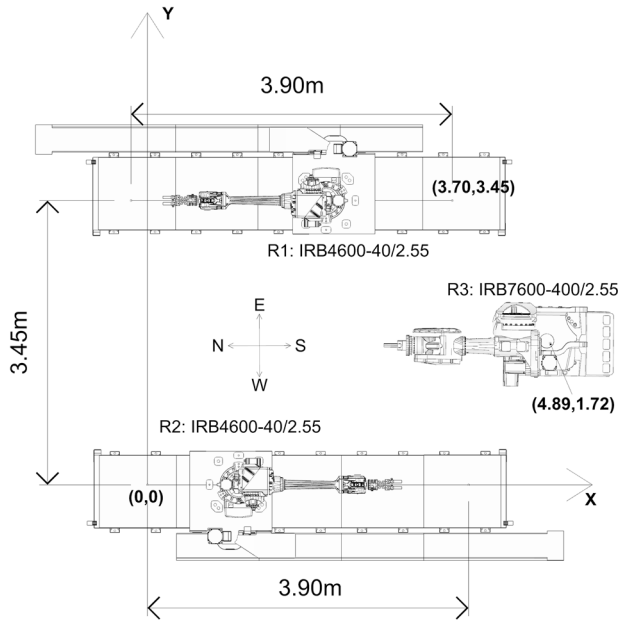

Fig. 1 Layout of the three-robot cooperative fabrication cell with North defined towards the left

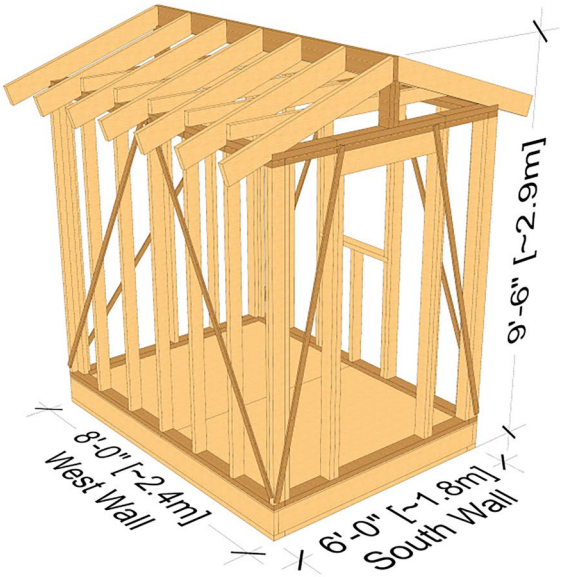

(a) Rendering of the structure showing the dimensions and naming convention for the walls.

(b) Image of structure showing its placement in the robotic work cell (from Bruun et al. (2022b))

Fig. 2 The prototype timber structure

Additionally, each of the IRB4600s is equipped with a high-definition 3D machine vision camera, the details of which are further discussed in Sect. 4.1.

The computational workflow relies on the COMPAS framework (Mele and others 2017). Robotic fabrication processes are planned and executed using the COMPAS FAB package in conjunction with a ROS backend (Rust et al. 2018). The execution of robotic motion commands is facilitated through COMPAS RRC (Fleischmann et al. 2020), and the corresponding RRC driver operates on the IRC5 controller.

3.2 Experimental prototype

At the heart of this research project is a prefabricated physical prototype - a timber shed structure constructed in accordance with conventional American stick frame construction practices. This prototype serves as a representative example of an existing structure that will undergo robotic disassembly and reassembly, demonstrating the real-world application of the computational methods developed in this research. Illustrated in Fig. 2, the structure has dimensions of 8×6 ft ($\sim 2.4 \times 1.8$ m) in plan, a stud wall height of 8.0 ft (~ 2.6 m), and a crown height of 9.6 ft (~ 2.9 m). Constructed using 2×4" and 2×6" SPF dimensional lumber, the traditional planar wall sheathing is replaced with linear members positioned diagonally across the stud wall to impart the necessary shear stiffness.

To streamline the forthcoming presentation of results and discussion regarding robotic fabrication sequences, the overall prototype structure is represented as a composite of distinct sub-structures - namely, the four walls (East, West, North, South) and the roof. Each of these sub-structures is then comprised of individual linear members, systematically labeled, and color-coded according to their respective types as shown in Table 1. The color-coded members and the five sub-structures are depicted in Fig. 3, where the individual members are labelled using the following convention *AB#_*, where:

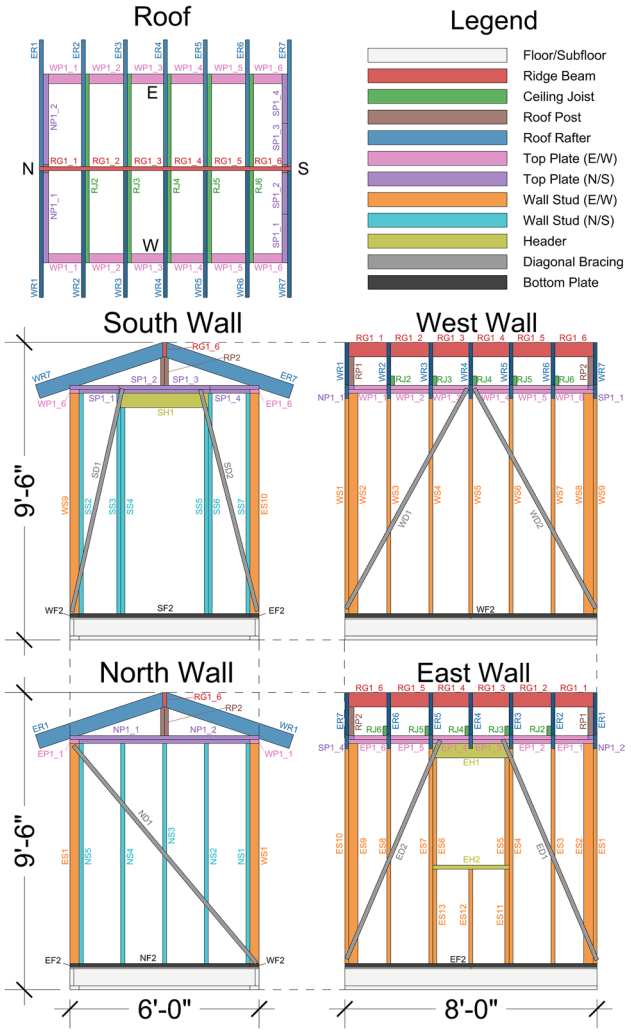

Fig. 3 Prototype structure shown as an assembly of five sub-structures with the members in each color-coded according to their type

A: The first letter indicates if it is part of the roof (R) or one of the four walls (N, S, E, W).
B: The second letter represents the type of member, as shown in the 2nd column of Table 1.
#: The third digit is used to number a unique member of a particular type.
$: The fourth digit (if required) is used to number a section of a single member.

The color-coding and member notation described in Table 1 and Fig. 3 matches the topological support hierarchy representation, which is introduced in Sect. 4.2. This convention is consistently used in all the subsequent results and discussions in the paper.

Table 1 Members in the prototype structure

Member	Letter	Count	Color
Floor	N/A	N/A	White
Roof girder	G	1	Red
Ceiling joist	J	5	Green
Roof post	P	2	Brown
Roof rafter	R	14	Blue
Top plate (E/W)	P	2	Pink
Top plate (N/S)	P	2	Purple
Wall stud (E/W)	S	22	Orange
Wall stud (N/S)	S	12	Cyan
Header	H	3	Yellow
Diagonal bracing	D	7	Grey
Bottom plate	F	4	Black

3.3 Project phases

The ZeroWaste project aims to develop an computational workflow for executing a cooperative, scaffold-free robotic disassembly and reassembly process on an unknown existing structure. The practical implementation of this goal involves a series of physical demonstrations of the prototype timber structure that was described in Sect. 3.2. The overall project is strategically divided into three distinct fabrication phases, each serving as a milestone to incrementally evaluate the developed methods that will be described in Sect. 4. Each phase demonstrates increasing complexity in both the structural disassembly and reassembly tasks and the degree of cooperative robotic sequencing necessary to execute these tasks in a scaffold-free manner. These phases are as follows: Phase 1, single target member removal; Phase 2, full wall disassembly and partial reassembly; Phase 3, full wall removal and reassembly. Further details and the results of these fabrication phases are presented in Sect. 5.

4 Workflow and methods

The overarching computational workflow utilized across all phases of the ZeroWaste project is illustrated in Fig. 4, depicting three primary components. Firstly, the use of 3D cameras mounted on robots to capture geometric and positional data pertaining to the unknown existing timber structure, which is here represented by the prototype shed (Sect. 4.1). Secondly, calculation of potential cooperative robotic disassembly and reassembly sequences when given user-specified member targets. This is achieved by leveraging the topological member support hierarchy representation of the structure (Sect. 4.2). Lastly, the workflow incorporates an evaluative process, assessing the feasibility of generated fabrication sequences, given the generated geometric data

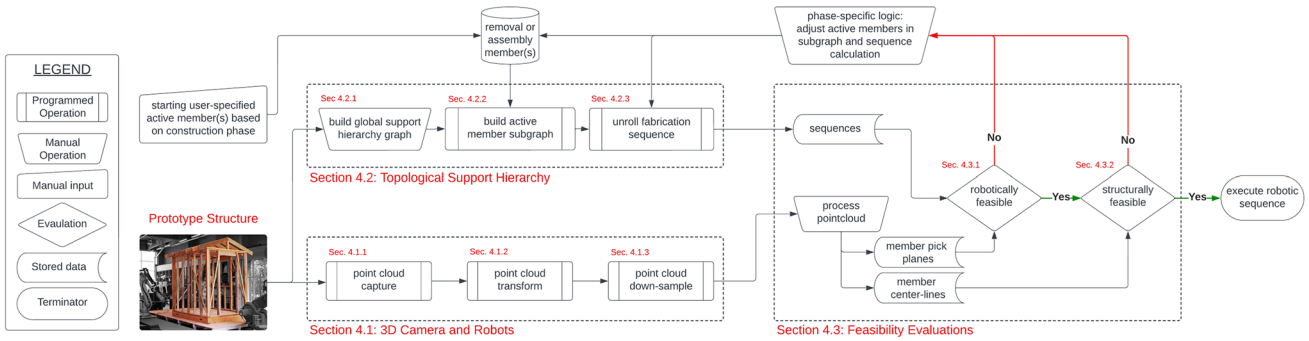

Fig. 4 Computational workflow showing the interaction between the methods described in Sect. 4

on the structure, regarding both structural performance and constraints associated with robotic reach and path planning (Sect. 4.3).

4.1 3D camera and robots

Each of the two IRB4600 robots, positioned on tracks, is equipped with a Zivid 3D structured light camera with a spatial resolution of 0.39 mm at a distance of 700 mm (Zivid AS 2021). The initial phase of the project involved creating a point cloud of the entire existing structure, which is a composite stitched together from several independent camera captures taken at various locations around the structure. Performing this procedure is essential before initiating any fabrication processes since an accurate digital representation of the as-built geometry of the unknown structure is required. Even if a pre-existing digital model of the structure is available, as is the case with our prototype structure, this point cloud step must still be performed as the as-built conditions of the structure invariably differ from the perfect digital model.

Moreover, beyond generating an accurate geometric representation of the structure, accurately positioning this geometry within the workcell is equally vital. This requires that the structure is correctly situated with respect to robots. Precise relative positioning is essential for the execution of robot move commands, which are sent relative to robots' base coordinate frame - that is, where the robot perceives its spatial location to be. Therefore, maintaining alignment between the as-built digital representation of the real structure and the perceived location of the robots in the fabrication cell is crucial for the execution of all robotic movements.

4.1.1 Point cloud capture

To construct an accurate as-built model of the structure, the robots capture 3D images from different spatial positions as they move around the structure (R1 = 105, R2 = 62 separate positions). Each capture generates a unique point cloud. The individual point clouds are then transformed to the correct global coordinate frame and combined into a single point cloud representing the whole structure, shown in Fig. 5.

4.1.2 Point cloud transform

The cameras are mounted on the robots used for the fabrication tasks, which is known as an eye-in-hand setup. Since the Tool Center Point (TCP) location with respect to the robot base is always known by the robot controller, this can be used to perform coordinate transforms on point clouds captured by the fixed camera. A point in the camera's coordinate system (i.e., how the camera sees the object), P_{object_camera}, can be transformed to a point in the global coordinate frame of the CAD model, P_{object_world0}, aligned with where the robots are situated in the global coordinate frame in the following manner:

$$P_{object\_world0} = H_3 * H_2 * H_1 * P_{object\_camera}$$

Where the 4x4 transformation matrices are the following:

H1: from TCP to camera. This transformation is calculated from a single eye-in-hand calibration routine that must be performed only once each time the camera is re-mounted.

H2: from robot base to TCP. This transformation is calculated from the positional frame representing the TCP, which is queried from the robot controller using the COMPAS RRC API (Fleischmann et al. 2020) at each camera capture.

H3: from World0 to Work Object (WOBJ) frame. This transformation is calculated from an user-defined coordinate frame set for each robot. This frame serves to establish a unified coordinate system for all the robots in multi-robot process, aligning them with the global coordinate

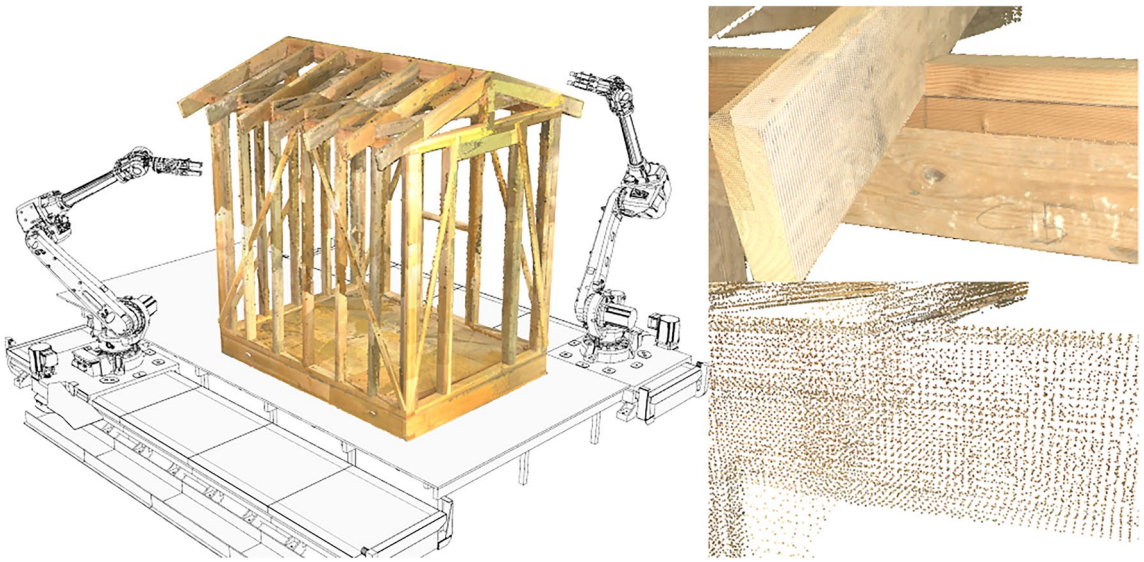

Fig. 5 As-built point cloud of the prototype structure from combined individual captures transformed to the correct location in space with respect to the robotic cell (left). Point cloud density for a small region of the structure before (top-right) and after (bottom-right) down-sampling with low-definition settings

frame of the CAD model. Consequently, all positional data is defined relative to this unified coordinate system.

4.1.3 Point cloud down-sample

The 3D cameras have a resolution that results in captured point clouds with greater fidelity than is strictly necessary for the subsequent robotic processes. Individual captures range from 50 to 200k points, resulting in raw combined point cloud model with 23.6M points (R1 = 14.5M and R2 = 9.1M points). A model of this size is computationally expensive to work with. In addition, the process of combining separate captures also leads to overlapping regions with duplicated points. Thus, further processing to reduce the overall point cloud density and remove the unnecessary duplicate points is required.

Table 2 Hyper-parameters and results for low-definition (LD) and high-definition (HD) down-sampling procedures

	LD	HD
pcd (start)	23.6M	23.6M
voxel_size (m)	0.010	0.001
nb_neighbor	30	20
std_ratio	1.0	2.0
nb_points	20	20
radius (m)	0.08	0.08
pcd (down-sample)	0.6M	11.8M
pcd (manual clean)	0.5M	11.3M

The raw point cloud undergoes down-sampling using statistical outlier, radius outlier, and voxel filters from the open3D package library (Zhou et al. 2018). The hyper-parameters for this process are shown in Table 2, where the low-definition (LD) settings result in a coarse overall model with only 0.55 million points, while the high-definition (HD) settings result in a model with 11.8M points. A final manual clean to remove unnecessary points, such as the ground, or any visible missed outliers, further reduces the model size slightly. The smaller LD model is used in computational processes where working with a minimal dataset is crucial, while the higher-quality HD model is suitable for visual applications.

Figure 5 displays the final combined model of the as-built prototype structure accurately located with respect to the robotic cell after the process of transformation and down-sampling. This image also illustrates the difference in the density between the raw and down-sampled point clouds for a small region of the structure.

4.2 Topological support hierarchy

Creating a computational framework to plan disassembly and reassembly sequences that are both stable and feasible requires a robust representation of the interconnections and support relationships within a structure. One effective method for visualizing this connectivity is using a multidirected graph (multidigraph) data structure Valiente (2021). In the context of this research, we developed a representation referred to as the topological support hierarchy graph. In this graph, individual members are depicted as vertices, while

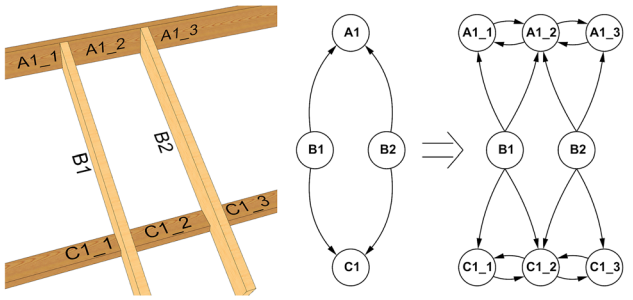

Fig. 6 Directed edges show that members B1, B2 are supported by members A1 and C1. These support members can also be shown subdivided into their constituent submembers that are connected with parallel and opposite edges to represent a fixed connection

physical connections between members are represented as edges. The direction of support is indicated by outgoing edges, effectively portraying the load-path.

However, representing geometric information, such as where along a member (e.g., a top plate) multiple members are being supported, poses a challenge in a topological data structure like a graph. To address this challenge, we propose a more detailed and precise graph representation by decomposing certain elements into their constituent submembers. Each submember is then treated as an independent vertex in the graph. To signify their mutually supportive relationship, vertices corresponding to submembers of the same member are connected by two parallel, opposing edges-a situation we refer to as a fixed connection.

Figure 6 illustrates the methodology for how a structure can be represented as a topological support hierarchy graph, for two members (B) supported by members (A and C). This graph representation can be further refined by dividing members A and C into submembers, providing a more nuanced depiction of how individual members are supported within the structure.

4.2.1 Build global support hierarchy graph

The global support hierarchy graph representing the entire prototype structure, which is an input to the computational processes for planning robotic fabrication sequences, is shown in Fig. 7. Constructed manually, this graph adheres to the principles illustrated in Fig. 6. Vertex names and colors are aligned with the member naming and color scheme described in Sect. 3.2, while edges are color-coded based on their originating vertices. To more accurately capture the support a hierarchy of the numerous individual members supported on them, the top plate and roof ridge beam members are represented as a series of submembers with fixed supports between them.

The graph in Fig. 7 visually partitions the structure into five distinct regions, either the roof or one of the four walls. However, this segmentation is primarily for clarity since the relative positioning of vertices lacks significance, as a graph data structure exclusively conveys topological information. The structure terminates at the foundation supports, visually shown in the graph by octagonal vertices that represent the connection between the bottom plate of each wall and the ground beneath.

4.2.2 Build active member subgraphs

Given an active member, such as a target specified for removal, an algorithmic operation can be executed on the global support member hierarchy graph of the entire structure. This procedure yields a subgraph encompassing the members that are directly affected during the removal of the active member.

This procedure is based on a customized breadth-first search algorithm (Valiente 2021), which is used to traverse the regions in the global support hierarchy graph adjacent to the vertex representing the target member. The rationale for this search approach is that achieving a feasible disassembly sequence without leaving unstable or disconnected components in the structure is higher when all members in the region connected to the target member are also removed or identified as requiring some form of temporary support during the overall removal process. For instance, if an active member is supporting several other members, it is logical to remove these supported members first as it is unlikely that they will remain structurally stable upon the removal of the active member. Thus, a breadth-first search is used to identify whether a member actively supports or is supported by other members, a condition represented by incoming and outgoing edges from neighboring vertices. Thus, any members connected to the active member will become part of the overall disassembly sequence. This procedure is then iterated to identify the members in turn supported by these intermediate members, resulting in a subgraph of the global support hierarchy graph that represents all the affected members in for a user-specified active member.

The process of calculating subgraphs for individual user-specified active members is shown in Algorithm 1, with the breadth-first search performed in the *calc_subg* function (Appendix A.1). When multiple user-specified active members are indicated for a single disassembly procedure, there is no need to repeat the breadth-first search. Instead, as shown in Algorithm 2, the subgraphs representing the individual members can be joined to produce the subgraph for the multiple active member case. All graph-based computational processes are performed using the NetworkX package for Python (Hagberg et al. 2008).

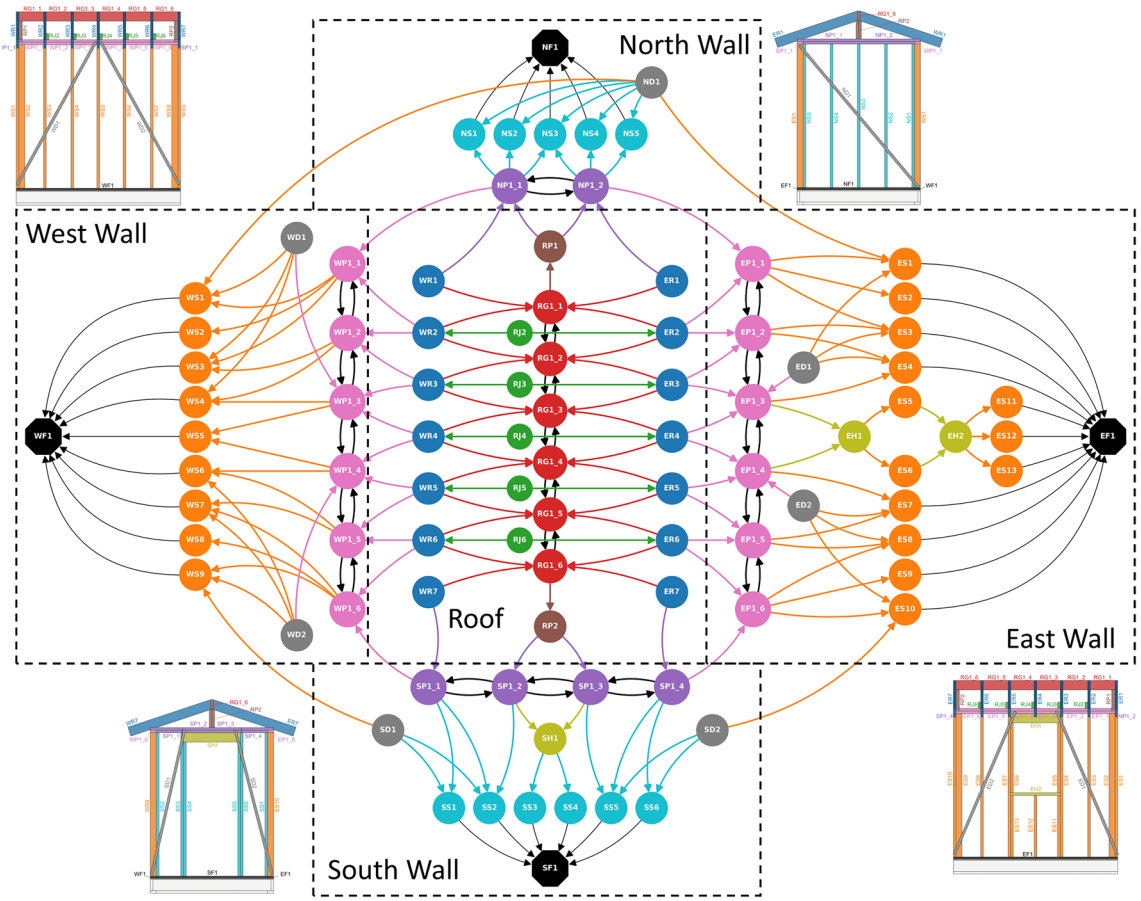

Fig. 7 The global connection hierarchy in the timber prototype structure is represented as a multidirected graph with outgoing edges indicating the direction of support. The graph is organized into five regions, where the names and colors of the vertices are based on the convention introduced in Sect. 3.2

Algorithm 1 Single Member Subgraph(s) Calc

```
procedure BLD_SUBG_SINGLE(G, rms)
    Ks ← []
    for rm in rms do
        K ← calc_subg(G.copy(), rm)
        n_cut ← fxd_nodes_cut(G, K)
        fxd_nodes_support(G, K, rm, n_cut)
        Ks.append(K)
    end for
    return Ks
end procedure
```

Algorithm 2 Multi-Member Subgraph Calc

```
procedure BLD_SUBG_MULTI(G, Ks, rms)
    K_joined ← nx.compose_all(Ks)
    add_in_extra_edge(G, K_joined)
    n_cut ← fxd_nodes_cut(G, K_joined)
    fxd_nodes_support(G, K_joined, rms, n_cut)
    return K_joined
end procedure
```

The breadth-first search concludes when the vertex-checking queue is empty. This occurs before traversing the entire graph due to certain conditions that lead to a vertex being labelled as an end, meaning its neighbors are not examined. For instance, a vertex with only outgoing edges implies that the member it represents can be removed without impacting any other parts of the structure. Conversely, a vertex with only incoming edges designates a foundation support vertex that will not be removed.

The end condition is also triggered for any vertex possessing at least one fixed edge (i.e., equal and opposite parallel edges), indicating that it represents a submember. However, additional logic is necessary to determine whether these submembers qualify as valid end supports. A submember with only one fixed connection, designating it as the terminal segment of a larger member, may pose a potential stability hazard and requires further scrutiny. If such a submember shares a sole unidirectional

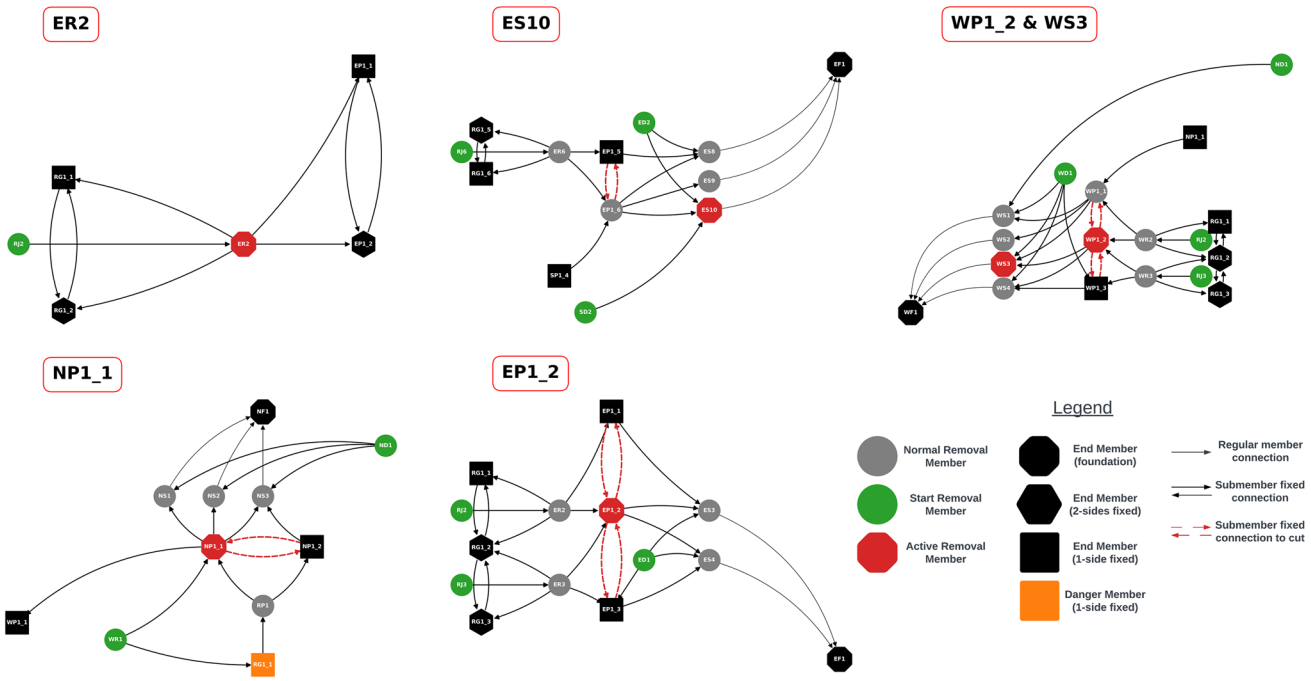

Fig. 8 Examples of active member subgraphs constructed using the algorithmic procedures described in Sect. 4.2.2. Vertices and edges are drawn to represent the different conditions as per the legend

edge with an active member, it necessitates removal, thus being treated as a standard vertex to be added to the breadth-first search queue. Alternatively, the submember may also require removal if all its edges are found in the subgraph, a condition verified in the *fxd_nodes_cut* function Appendix A.2). Otherwise, the submember is considered adequately supported and remains in the structure acting as an end support in the subgraph.

In the *fxd_nodes_support* function, all the ends that remain in the structure (i.e., submembers with fixed connections) are checked for adequate support at the culmination of the removal process (Appendix A.2). Adequate support is defined by the requirement that at least two supports (i.e., outgoing edges) persist in the global support hierarchy graph once the subgraph has been deleted. For example, a submember with two fixed connections, signifying its placement within the interior of a larger member, is considered adequately supported. This condition serves as a safeguard against the formation of structurally undesirable cantilevered segments within the remaining structure after the disassembly process is completed. This is checked in both the single and multi-member subgraph procedures outlined in Algorithms 1 and 2.

Figure 8 shows example subgraphs calculated using the computational procedures outlined in this section given different user-specified targets: east side rafter #2 (ER2), east side stud #10 (ES10), north side top plate submember #1 (NP1_1), east side top plate submember #2 (EP1_2), and the composite of west side stud #3 (WS3) + west top plate submember #2 (WP1_2). The colors for the edges and vertices in these subgraphs no longer indicate the physical member type, but instead represent output related to how the edges and vertices have been labelled in the computational process when generating the subgraph. For example, black is used for end members and green is used for start members. The shape of the vertices is also used to distinguish between different conditions. If an edge is black it represents typical support between members, but dashed red edges indicate that a submember will require physical cutting from the overall member it is a part since it must be removed in the disassembly process. The complete legend for the nodes and edges are labelled in the active member subgraphs is shown in Fig. 8.

4.2.3 Calculate fabrication sequences

A computational procedure is employed to calculate a set of potential fabrication sequences, utilizing an active member subgraph generated through the methodology outlined in

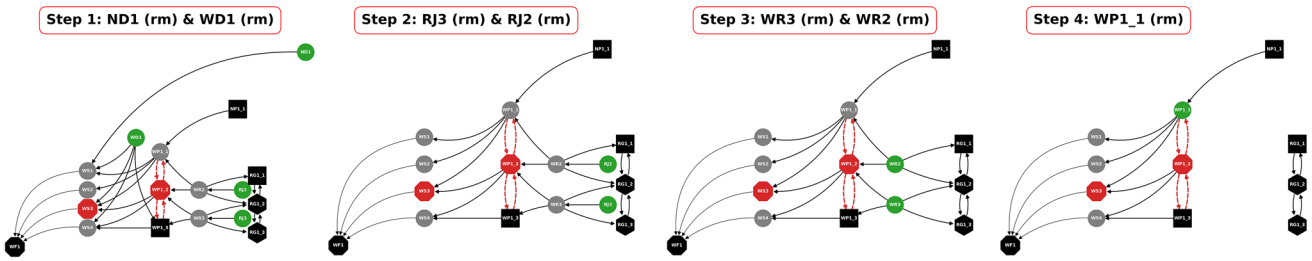

Fig. 9 Example of a partial disassembly sequence (four steps) calculated from the subgraph for active members WP1_2 & WS3. After each step, the subgraph is relabeled with new start nodes in green

Sect. 4.2.2. Conceptually, this involves unfolding the subgraph data structure into a linear sequence of discrete fabrication steps. The overarching method for generating these sequences is summarized in Algorithm 3, with supplementary functions further explained in the Appendix (Appendix A.3).

Algorithm 3 Unroll subgraph into sequence

```
procedure BLD_SEQUENCE(K, rms, num_agents)
    saved_K, saved_seq ← [],[]
    n_active_type ← ["start","rob_sprt"]

    while True do
        n1 ← find_n_active(K, n_active_type)
        n2 ← set_new_to_rob_support(K)

        if n1 ∪ n2 is ∅ then
            terminate loop
        end if

        n_rmv,n_rob_sprt ← select_n_active(n1,n2)

        saved_K.append(K)
        saved_seq.append(n_rmv)

        K.remove_nodes_from(n_rmv)
        K ← new_subg_relabel(K, rms)
    end while
    return saved_K, saved_seq
end procedure
```

The algorithm locates start vertices in the subgraph describing the full fabrication sequence. These vertices are first saved as a discrete disassembly step and then removed from the subgraph to represent the physical process occurring. The remaining subgraph is then relabeled with new start nodes to account for the resulting changes in the support hierarchy after this step is executed. This process of locating, removing, relabeling is iterated on the subgraph until all nodes are removed. The objective is to optimize the removal of the maximum number of members in a single step, corresponding to the available robotic agents. In cases where the number of start nodes exceeds the count of robotic agents at a given step, a sequence is generated for each permutation. Subsequently, this exhaustive set of sequences is evaluated as outlined in Sect. 4.3, to ascertain feasibility in terms of structural behavior and robotic reachability.

Figure 9 illustrates a representative outcome of the fabrication sequence calculation process applied to the WP1_2 & WS3 active member subgraph, which was shown in Fig. 8. These calculations consider the presence of two robotic agents, thus allowing the removal of a maximum of two members per step. In step #1, more than two start vertices are identified, implying the existence of multiple permutations at this stage, where the displayed sequence represents just one of these possibilities. All end nodes (depicted in black) are retained in the sequence graphs for better visualization; these nodes are not isolated components but are interconnected and adequately supported by the remaining structure beyond the boundaries of the specific subgraph.

4.3 Feasibility evaluations

The computational methods discussed in the preceding Sect. 4.2, rooted in the topological support hierarchy representation of the structure, generate a sequence of fabrication plans when provided with a set of active members. The primary goal at this stage is just to discern fabrication sequences that could potentially be executed without external scaffolding while ensuring structural stability. Subsequently, these candidate sequences must undergo further examination, considering the physical structure itself, to verify feasibility and identify the optimal sequence.

An analysis of the generated sequences, evaluating both structural and robotic feasibility, precedes the selection of a sequence for execution. The verification process involves two concurrent procedures applied to the accurate as-built point cloud gathered as per the methods described in Sect. 4.1. Firstly, the validation of robotic path planning and reachability is conducted using the COMPAS and COMPAS FAB package with a ROS backend (Rust et al. 2018; Mele and others 2017). Secondly, a parametric finite element (FE) analysis of the structure is carried out in Rhino/Grasshopper with Karamba3D (Rutten 2007; Preisinger and Heimrath

2014) to assess the structural behavior at each step in the fabrication sequence.

4.3.1 Robotic feasibility

The first procedure involves assessing the physical executability of a proposed sequence from the robotic perspective. This evaluation focuses on ascertaining whether a robot can safely access and grip each building member specified in the sequence. This assessment is performed computationally through an inverse kinematic (IK) path planning operation, trying to move the robot to a target location on a specified member in the structure. This is done using the *Plan Motion* script implementing the RRT-connect path planning algorithm available as part of the COMPAS FAB computational package (Rust et al. 2018). Generating a successful result from this operation ensures that the member is within the robot's reach. Furthermore, it confirms the existence of a feasible motion path from the initial position to the final target plane for the robot's TCP, avoiding collisions with itself, other robots in the work cell, the ground, or any part of the existing structure.

To ensure realistic outcomes, accurate information about the as-built conditions of the structure is essential. Consequently, the as-built point cloud of the structure serves a dual purpose: it is utilized to establish authentic pick locations on the members and to define precise locations for collision meshes in the IK checks. The point cloud undergoes an initial manual processing phase, where the user selects multiple sets of three points from various locations along members, used to build planes in space. These planes represent potential locations and orientations for a robot to move and grasp a member during the execution of a planned sequence.

An illustrative example of the entire process is depicted in Fig. 10. The X1 point designates the plane's center, serving as the target for the robot's TCP to move to. The orientation of the X-axis of the gripper is defined by the vector between X1 and X2. Y1, representing the third point on the member's surface, is necessary for establishing the spatial orientation of the plane. These designated pick locations are saved in a list and then undergo sequential testing during the evaluation of the disassembly sequence to assess which can be reached in a collision-free manner. If the IK checks return failure for all pick locations on a member, indicating the impossibility of the robot reaching this member from a path planning perspective, adjustments are necessary to the original disassembly sequence. These adjustments may entail removing additional members before attempting to remove a target member or repositioning the robots strategically during the sequence to minimize obstructions.

4.3.2 Structural feasibility

The second step involves an assessment of the structural performance throughout a potential disassembly and assembly sequence. This evaluation is conducted through a linear elastic FE model representing snapshots of the structure at various stages during the execution of a sequence. Like the robotic feasibility check, the as-built point cloud is employed to create an accurate FE model, ensuring its fidelity to the

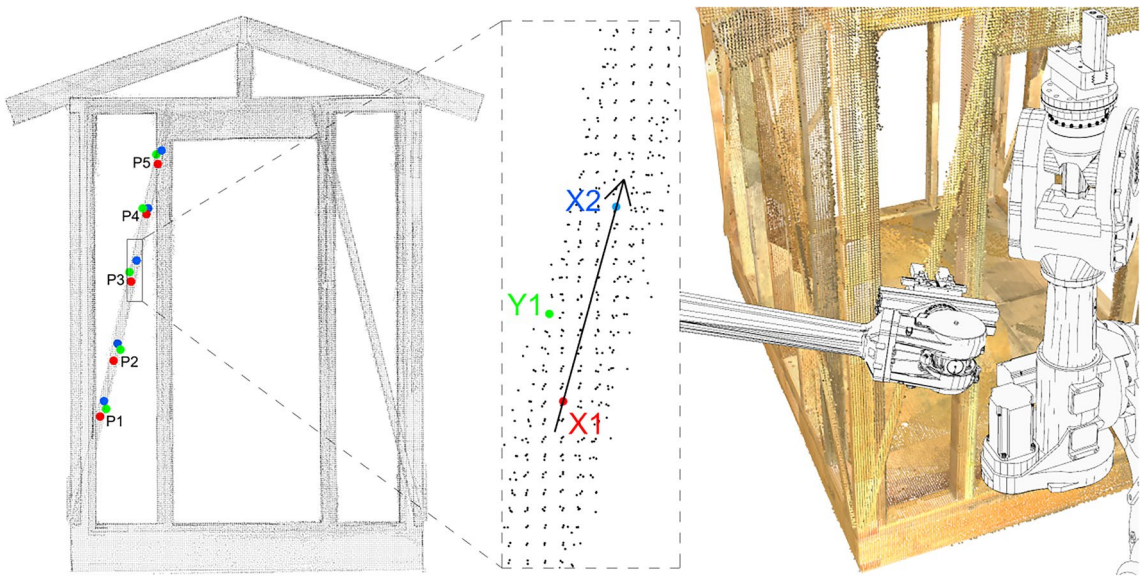

Fig. 10 Left: Five pick locations (P1–P5) on a member are manually initialized from the as-built point cloud of the structure. Middle: At each location, three points are used to define a spatial plane for the robot to reach. Right: Inverse kinematic path planning checks reveal that only P3 is reachable by a robot without encountering collisions with the structure or other robots in the work cell

real geometry of the structure. The beam elements in the model are located based on the center-line data of the members identified within the point cloud.

Utilizing the parametric Rhino/Grasshopper environment alongside the Karamba3D finite element package (Rutten 2007; Preisinger and Heimrath 2014) allows for the rapid investigation of candidate fabrication sequences. In this parametric environment, members can be selectively activated or deactivated to reflect a fabrication sequence being executed. Furthermore, additional supports, reflecting the positions of the robotic arms gripping the structure during the execution of a sequence, can be toggled on and off. This temporary support provided by the robots is represented as a standard pin support in the model. The structural members are themselves modeled as beam elements with semi-rigid joint connections. The overall FE model terminates at the bottom of the stud members, where their connection to the bottom plate is represented with a pin support.

While the actual structure only experiences self-weight loading, based on a dimensional lumber density of 6 kN/m^3, a more realistic loading condition is simulated by applying an additional uniform roof loading of 2.0 *kPa* distributed across the roof area. To further emulate real-world conditions, a vertical load of 1.0 *kPa* is applied to the wall studs, representing the typical presence of hanging cladding and plywood sheathing in such structures.

The structural assessment fails if, at any step a given fabrication sequence, either the strength or serviceability conditions are exceeded. These conditions are calculated with the conservative assumption that SPF stud grade lumber is used, which has a bending strength of 4.3 MPa and a modulus of elasticity of 3 GPa (American Wood Council 2015). The user-specified strength condition dictates that no member should experience a combined bending and axial stress exceeding 3 MPa. Additionally, the serviceability condition stipulates that beam deflections should not surpass 2 L/360, L/360, or L/180 for fixed, simply supported, and cantilever situations, respectively.

4.4 Physical implementation

After calculating a feasible fabrication sequence, the planned robotic path for each step in the sequence is sent from the human operator's computer to the robotic controller. The execution of each step begins when the human operator presses the play button on the Flex Pendant interface connected to the controller. For the removal of a structural member, the planned path starts from the initial resting position of the robotic arm and ends on the targeted member. The pneumatic gripper is then engaged to securely grasp the member. At this point, the robotic sequence pauses, requiring the human operator to manually remove any nail fasteners. This task is performed using a reciprocating saw equipped with a metal cutting blade. Additionally, any fixed members can be cut into sub-members at this stage. Once the structural member to be removed at that specific step is freed and prepared for removal, the human operator triggers the start of the removal path. This process is repeated several times throughout a fabrication phase, alternating which robots are used to temporarily support the structure and to place/remove members.

5 Results and discussion

In the following section, the planning and execution of three distinct fabrication phases are documented. The overall project is strategically divided into three phases to incrementally test the developed methods outlined in Sect. 4. Each phase increases the complexity of the structural disassembly and reassembly tasks, as well as the degree of cooperative robotic sequencing required for execution. All phases are to be planned and then executed in such a way that the structure not only remains stable throughout the fabrication process but the resulting final structure also terminates in a state that is stable.

5.1 Phase 1 (P1): single target member removal

The first phase focuses on validating the overall computational workflow developed for the project. Tasked with a straightforward fabrication objective, P1 demonstrates robotic sequence planning and execution where the starting goal is simply to remove a single simulated "damaged" member from the prototype structure. The cooperative robotic process involves two of the three available robots (R2 & R3), which is the minimum required for the robotic workflow to be considered cooperative. The planning of this phase was discussed in an existing work-in-progress paper on the project (Bruun et al. 2022b), with additional information on the planning and execution of the phase presented in this paper.

5.1.1 Preliminary planning

Member SS1 (South Wall, Stud #1) is chosen as the member that is the target to be removed in P1. The active member disassembly subgraph for SS1 with all corresponding elements highlighted on the structure is shown in Fig. 11a.

A potential four-step disassembly sequence generated from this subgraph is shown in Fig. 11b. The structural and robotic kinematic feasibility evaluation reveals that the sequence is structurally feasible but fails since no robot can reach member SS1 without colliding with either member WS9 or SS3 in its path. Thus, this first iteration indicates

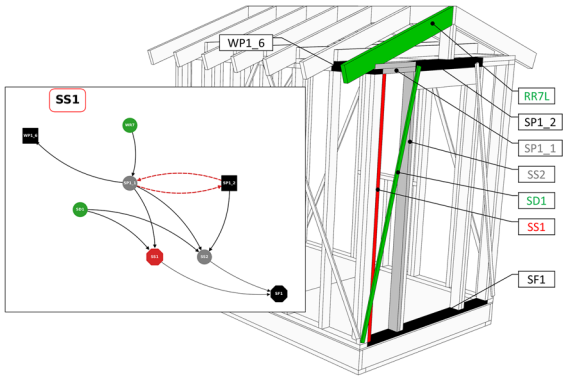

(a) active member subgraph for member SS1

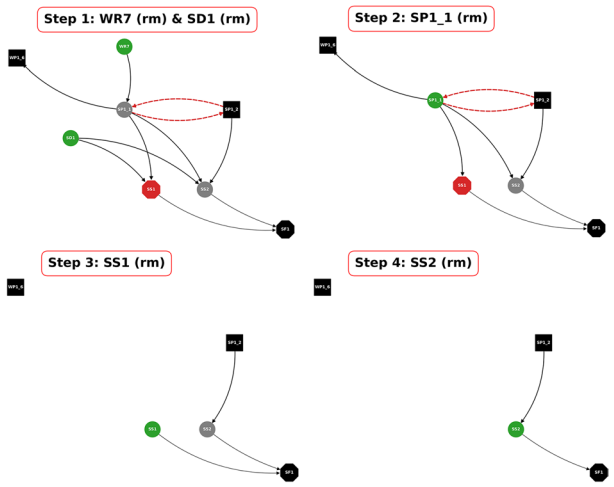

(b) potential disassembly sequence

Fig. 11 Planning the removal of member SS1

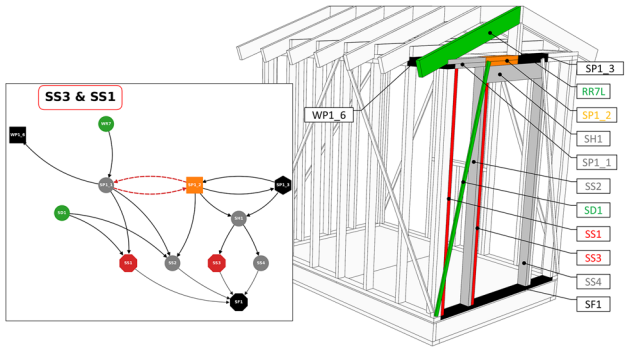

(a) option 1: adding SS3

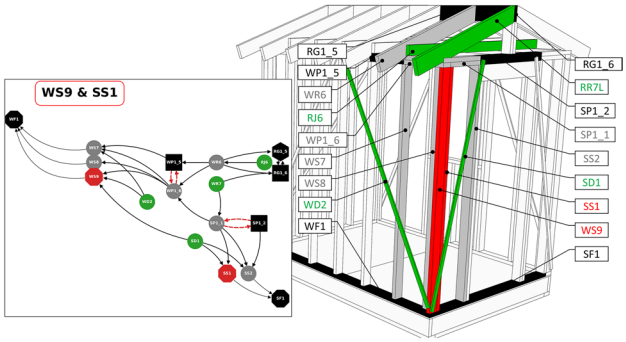

(b) option 2: adding WS9

Fig. 12 Two new active member subgraphs generated from the inclusion of additional removal targets determined by the feasibility evaluation for the planned removal of SS1

that the removal of either WS9 or SS3 must first occur as part of the overall fabrication task. This results in the generation of two new subgraphs representing the affected region of the structure when either of these members is added as an active member.

In Fig. 12a, the subgraph for option 1 is presented, involving the removal of SS3 before SS1. This option requires the removal of a total of 9 members but leads to inadequate support for member SP1_2 upon the termination of the sequence. On the other hand, Fig. 12b depicts the subgraph for option 2, removing WS9 before SS1. Despite a more extensive removal process involving 12 members, this option ensures a stable structure at the end of the sequence. Consequently, option 2 is chosen for P1.

5.1.2 Fabrication sequence

Assuming the availability of two robotic agents for executing the planned fabrication task, a viable disassembly sequence is derived from the active member subgraph generated for option 2 (members WS9 and SS1). This computed disassembly sequence encompasses 9 discrete steps, wherein one or two members in the subgraph are safely removed from the structure using robotic agents. The actions in each step are determined based on the current state of the structure, visually represented by an updating subgraph at each step. The progression of the sequence and the planned action at each specific step is illustrated in Fig. 13a. Simultaneously, renderings of the structure, highlighting the targeted members for removal/support at that step and depicting the robots in the correct position for execution, are presented in Fig. 13b. In these figures, the pink denotes members that are temporarily physically

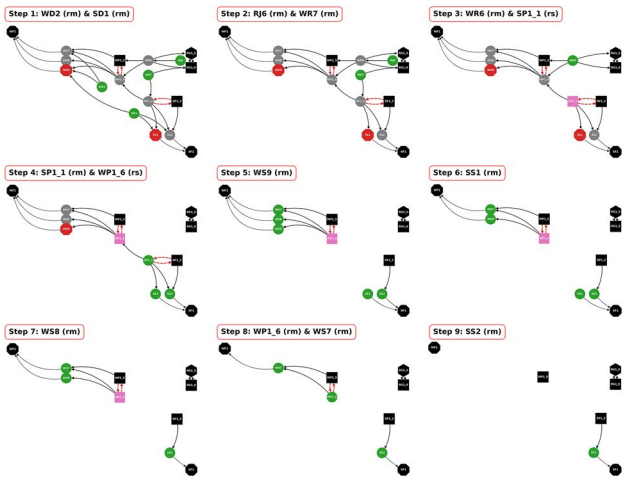

(a) sequence subgraphs

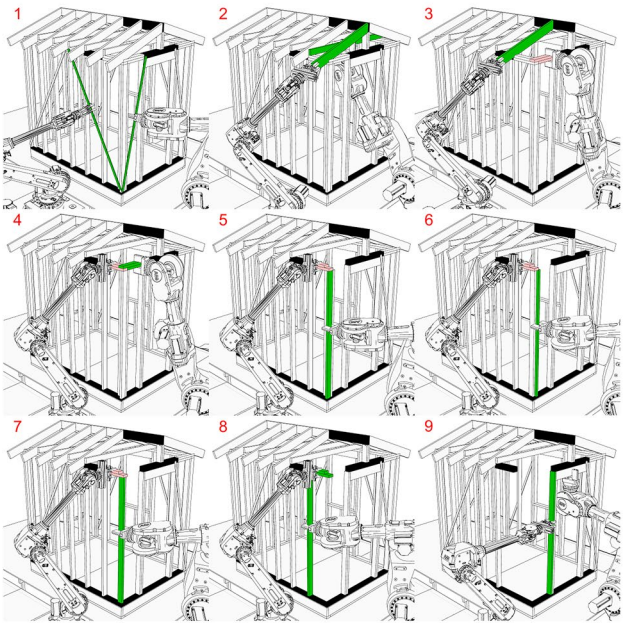

(b) sequence renderings

Fig. 13 Phase 1 disassembly sequence

supported by a robot, ensuring adequate stability during that step.

5.1.3 Execution and resulting structure

The resulting structure after the completion of this 9-step disassembly sequence is displayed in Fig. 14. Further snapshots of the structure and robots at various stages of the phase are provided in Appendix B.1, with a supplementary video clip demonstrating a subset of Phase 1 fabrication provided together with this paper.

5.2 Phase 2 (P2): full wall disassembly and partial reassembly

Building upon the methodologies explored in the initial phase, the second phase of the study extends the disassembly goal beyond a single-member target, as seen in P1. In P2, the objective is to safely remove a larger and more geometrically complex portion of the remaining South wall of the structure. This phase also introduces increased complexity in robotic planning by engaging all three available robots throughout the planned sequence.

In P2 the scope of the overall fabrication process is broadened by incorporating structural reassembly after completing the disassembly phase. This serves as a practical test for the reuse of members removed from the structure for alternative purposes. The disassembly goal in P2 is meant to explore what can be done when achieving a structurally sound final structure after disassembly is not possible without external support. Unlike P1, where a small disassembly intervention meant that finding a feasible sequence resulting in a stable final structure was possible, P2 involves a much larger and more complex disassembly operation where no safe resulting structure is identified within reasonable constraints (i.e., without calculating a sequence to dismantle the entire structure).

Thus, following the completion of disassembly in P2, the only viable means to safely conclude the process is either to provide external temporary support structures at the targeted location or to reuse several removed members to reassemble a new but simple supporting structure. Notably, this reassembly is considered partial, meaning that not all initially removed members are incorporated into the new structure. Additionally, in P2, the specific configuration of the new structure is not optimized; it solely acts as a prop, providing basic structural support to a region of the structure deemed unsafe after the disassembly is completed.

5.2.1 Preliminary planning

To facilitate the removal of the entire South wall, the members chosen include the remaining top plate members SP1_2, SP1_3, and SP1_4. This selection forms the disassembly subgraph depicted in Fig. 15a. Like the preceding phase (P1), the resultant disassembly sequence proves infeasible due to unavoidable collisions, particularly with member ES10. To address this challenge, as illustrated in Fig. 15b, ES10 is incorporated as a removal target prior to dismantling the top plate. However, this adjustment also yields an unsatisfactory sequence, revealing inadequate support for the ridge beam member RG1_6 upon completion of the disassembly process.

To rectify this structural instability, RG1_6 is included in the disassembly sequence, leading to the configuration

shown in Fig. 15c. Yet, the removal of RG1_6 fails to resolve the issue, as the instability concern is transferred to the subsequent member, RG1_5. Upon further examination, it becomes evident that achieving stability necessitates the removal of the entire ridge beam, along with all roof girders and joists. However, such an extensive intervention exceeds the intended scope of disassembly. Consequently, the disassembly process is limited to the members highlighted in the structure as shown in Fig. 15c, requiring a subsequent reassembly phase with additional support provided to stabilize member RG1_5 at the conclusion of the sequence.

5.2.2 Fabrication sequence

Assuming the availability of all three robotic agents for executing the planned fabrication task, a viable disassembly sequence is calculated for the disassembly subgraph shown in Fig. 15c. The progression of the sequence and the planned action at each specific step is illustrated in Fig. 16a. Simultaneously, renderings of the structure, highlighting the targeted members for removal/support at that step and depicting the robots in the correct position for execution, are presented in Fig. 16b. In these figures, the pink denotes members that are temporarily physically supported by a robot, ensuring adequate stability during that step.

The disassembly sequence unfolds through steps 1 to 8, reminiscent of P1, employing only two robots. However, from step 9 onwards, the involvement of all three robots becomes necessary, orchestrating a leapfrogging strategy to dismantle the members supporting the roof girder. In step 12 the structure is shown in its temporary state, stabilized by R3. At this point, further disassembly is hindered, given that only R3 can access the final members but R3 must concurrently support the structure at this step. In addition, RG1_5 will eventually require additional support at the conclusion of the disassembly as noted when planning this sequence. To address both challenges, a reassembly stage is initiated after step 12.

Several recently removed members—namely ER6, ER7, SS6, SS4, and SS4—are strategically reassembled into a new supporting structure as shown in steps 13 to 17 in Fig. 17. This new structure not only provides crucial support to member RG1_5 but also frees R3 since it is no longer required for support and can thus continue with the remaining disassembly steps. The final members are removed by R3 in steps 17 and 18, completing the planned disassembly sequence while resulting in a structurally sound final configuration.

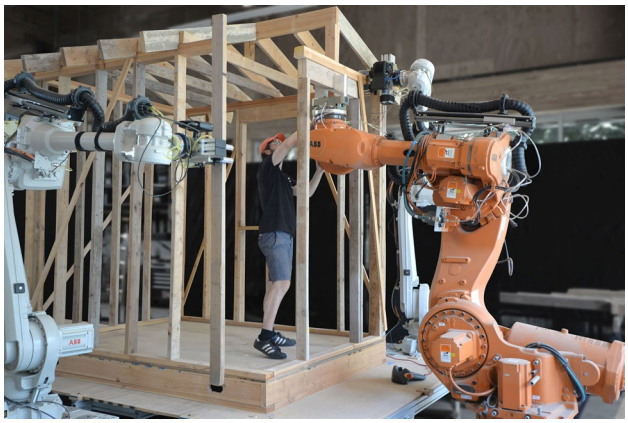

Fig. 14 Prototype structure at the end of the disassembly in Phase 1 (from Bruun et al. (2022b))

5.2.3 Execution and resulting structure

Figure 18 shows snapshots of the disassembly sequence at two critical steps. In step 10, all three robots are required. In step 12, R3 is used to support the roof girder before the reassembly begins and additional support is added to the structure.

The completed structure resulting from the reassembly sequence is shown in Fig. 19a. Additional snapshots illustrating various steps during disassembly and reassembly are presented in Appendix B.2, with a supplementary video clip demonstrating a subset of the Phase 2 fabrication provided together with this paper. Upon concluding Phase 2, in preparation for subsequent phases, the point cloud gathering procedure outlined in Sect. 4.1 is repeated to capture deformations in the structure and the as-built position of the newly added members. This updated point cloud and the assembly hierarchy graph are shown in Fig. 19b.

5.3 Phase 3 (P3): full wall and roof disassembly and reassembly

Phase 3 marks the project's culmination, surpassing the disassembly scopes of P1 and P2. In P3 the objective is to remove all remaining members in the West wall and roof sub-structures. Additionally, it introduces tighter constraints in reassembly, adopting a one-to-one approach: each extracted member is reincorporated to reshape the West wall into a lattice structure, improving its overall lateral stiffness.

5.3.1 Preliminary planning

As illustrated in Fig. 20, Phase 3 designates twelve remaining members within the West wall and roof sub-structures for removal. The diagonal brace (WD1), is also planned

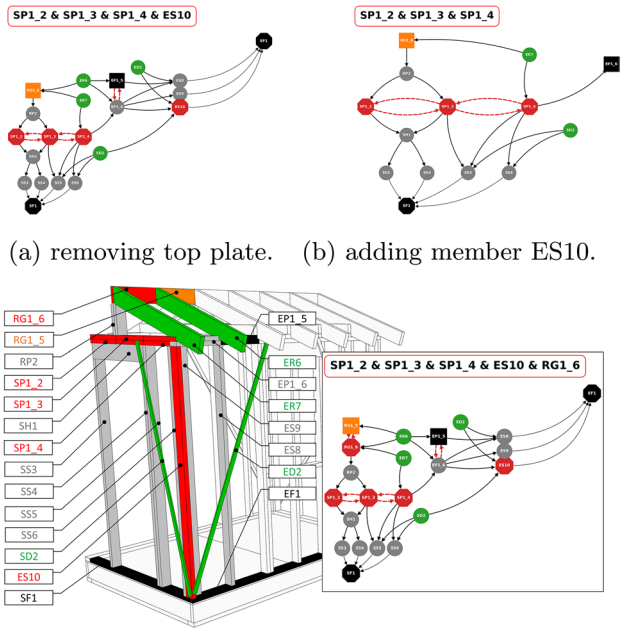

(a) removing top plate. (b) adding member ES10.

(c) final disassembly subgraph when adding RG1_6.

Fig. 15 Planning the removal of the south wall as part of Phase 2 and resulting in a final structure that requires additional support

for removal, but is not considered a valid member for reuse since the diagonal members take the place of typical planar sheathing used to provide lateral stiffness.

Only the two stud members in the North corner (WS1 and WS2) and the top plate (WP1) are not specified as removal targets. Retaining the corner stud members prevents the need to extend the disassembly sequence into the North wall, while the top plate acts as a support constraint for the newly reassembled wall. The planned goal for the reassembly process in P3 is to fit the new lattice wall structure within the current volume of the existing wall. This means that all the new members must fit within the original 4" thickness specified by the stud members in the wall (i.e., for a 2×4" stud wall).

5.3.2 Fabrication sequence

The disassembly and reassembly of the twelve specified target members results in a fabrication sequence consisting of 25 steps. This sequence can be represented as two distinct sub-tasks: (1) Steps 1–12 involve the removal and reassembly of the initial set of 6 members, while (2) Steps 14–25 involve the removal and reassembly of the subsequent set of 6 members. The first set consists members WS6, RJ5, WR5, RJ4, WR4, and WS5 (in order) and the second set consists of members RJ3, WR3, WS4, RJ2, WR2, WS3 (in order).

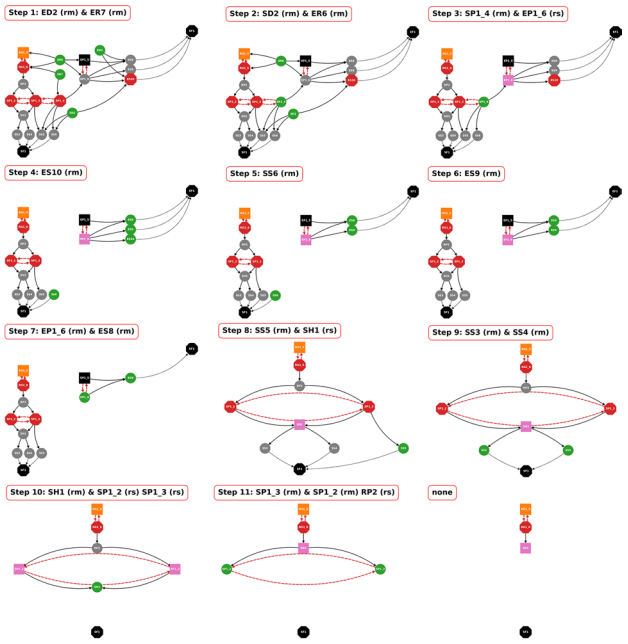

(a) sequence subgraphs

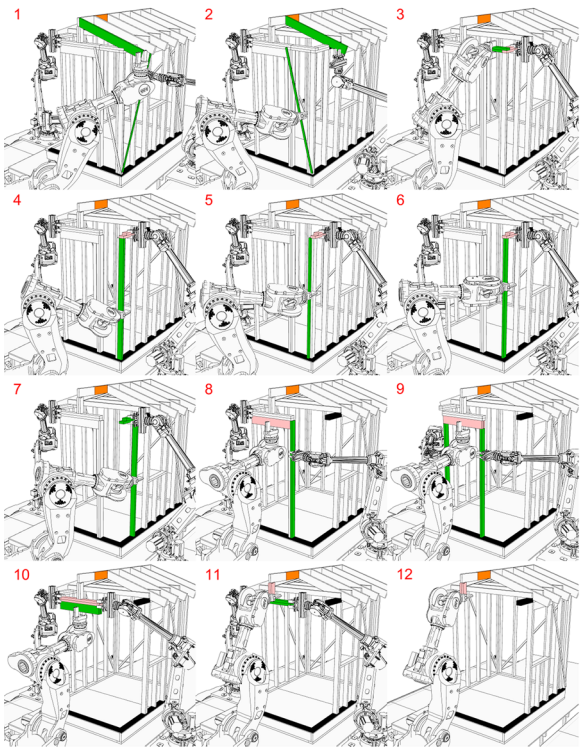

(b) sequence renderings

Fig. 16 Phase 2 disassembly sequence

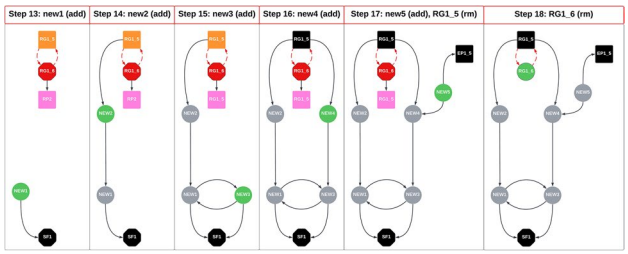

(a) sequence subgraphs

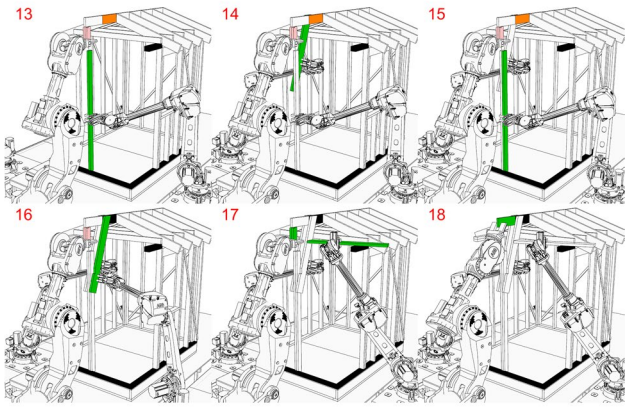

(b) sequence renderings

Fig. 17 Phase 2 reassembly sequence

In Fig. 21, the planned fabrication sequence is shown as a series of renderings of the structure at each step, highlighting the remaining members in the structure still requiring removal/support, the newly placed members, and the position of the robots involved in each step. Upon reassembly into the structure, the members are depicted in white, signifying that they are no longer part of the active sequence plan. To streamline the presentation within the main body of the paper, the corresponding support hierarchy subgraphs for each step are provided in Appendix B.3. Step 13, which is omitted from Fig. 21, represents the removal of the diagonal member (WD1), which as previously established is just a placeholder element used in lieu of planar sheathing. In steps 6/7 and 18/19, the robot first removes the roof joist, which frees the roof girder, then the joist is reattached to the top plate. In both the renderings and subgraphs, the pink denotes members temporarily supported by a robot, providing the necessary stability during the execution of the sequence.

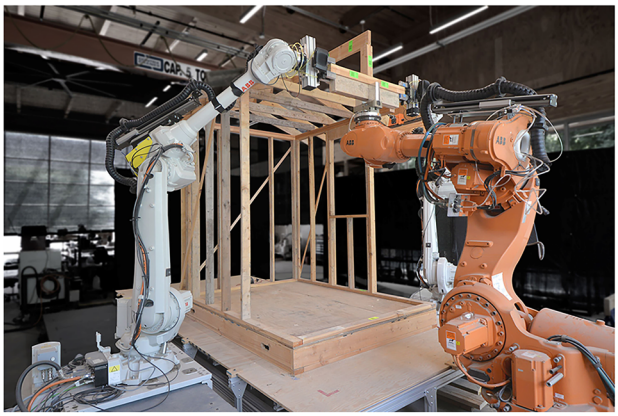

(a) Step 10 in the disassembly sequence. R3 is ready to remove SH1, while R1 and R2 support SP1_2 and SP1_3 respectively (from (blinded) .

(b) Step 12 in the disassembly sequence. R3 is supporting the remaining roof structure before the start of the reassembly sequence to add additional support.

Fig. 18 Snapshots of Phase 2 disassembly

5.3.3 Execution and resulting structure

Figure 22a shows a snapshot of the newly assembled structure at the end of step 24, as R2 is positioning the final planar element into the wall. Four of the reassembled members (e.g., RJ4, RJ5, RJ2, WR2) are placed in the out-of-plane direction to provide bracing to the wall, thus the planar wall itself consists of only eight new members. As shown in Fig. 22b the result is a planar wall where the standard vertical stud wall typology is replaced with a lattice typology. The lattice arrangement features members crossing at several points. At each of these points, the members are connected to each other to stiffen the entire wall system. The members are arranged along their strong axis, meaning that the thickness of the plane

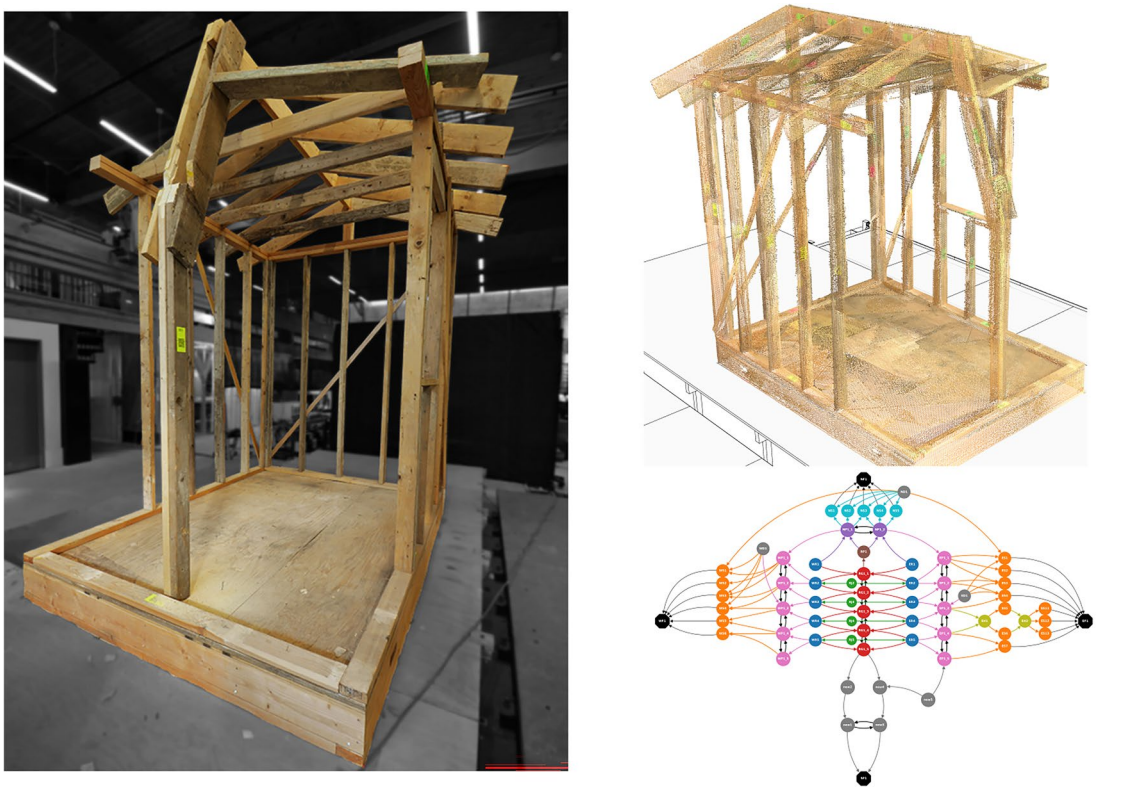

(a) Prototype structure. (b) As-built pointcloud and assembly hierarchy graph.

Fig. 19 The prototype structure at the end of the disassembly and reassembly in Phase 2

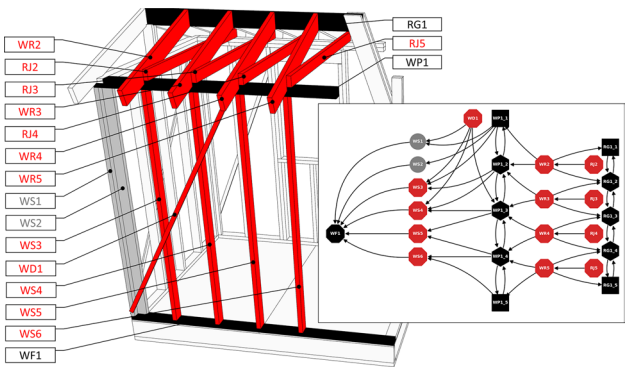

Fig. 20 The disassembly subgraph for the removal of the West wall and roof members

of the wall is only 2", thus two members can cross and still fit within the original 4" wall cavity as specified by the original wall studs. Additional snapshots illustrating various steps during disassembly and reassembly are presented in Appendix B.3, with a supplementary video clip demonstrating a subset of the Phase 3 fabrication provided together with this paper.

Two linear elastic finite element analyses were conducted to compare the relative lateral stiffness of the original and reassembled West wall. Despite the mass increasing from 34.4 to 44.1 kg between the original and reassembled wall, a significant improvement in stiffness was noted. For instance, the unbraced original wall with vertical studs exhibited a maximum deflection at its top of 67.6 cm, whereas the reassembled wall with a lattice configuration experienced a lateral deflection of only 0.3 cm. This comparison was solely intended for relative assessment, thus the applied lateral loading of 5 kN at the top of the walls was arbitrarily chosen. Additionally, to ensure comparability, identical support conditions were maintained across the models, with supports modeled as pins and connections between members fixed. Representing joints in a traditional stud wall as fixed is a conservative assumption since these connections are typically more flexible, suggesting that the actual performance of the traditional wall might be even worse if flexibility were introduced in the joints. The successful reassembly of the

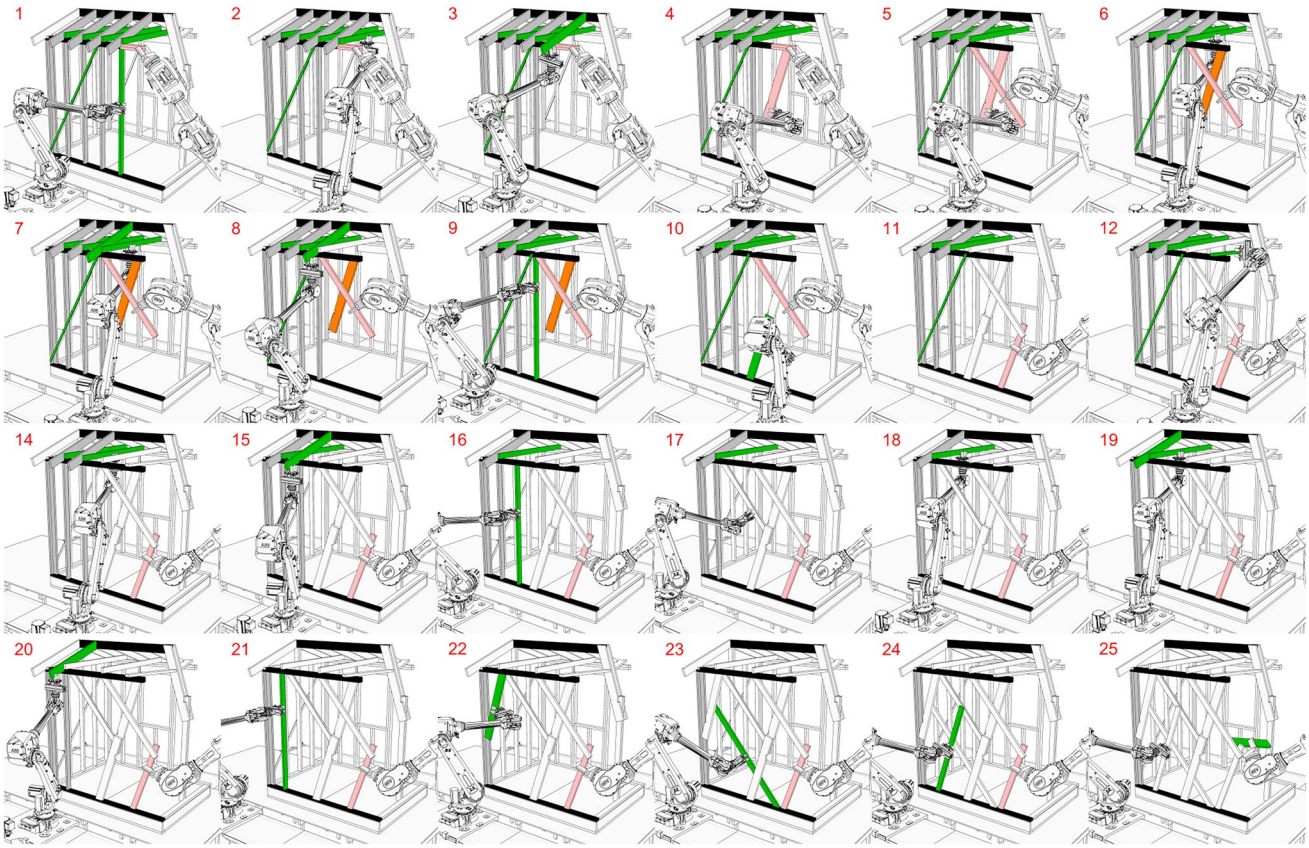

Fig. 21 Phase 3 disassembly and full reassembly (each member removed is reused)

West wall in Phase 3 demonstrated the potential for rebuilding a structure with enhanced structural performance.

Figure 23 summarizes the results of the finite element analyses, visually depicting the relative difference in deflection between the two configurations. While conventional stud walls typically rely on planar sheathing elements for lateral stiffness, advancements in digital fabrication raise questions about the necessity of this approach. Precise placement of elements in space allows for the exploration of alternative geometries beyond conventional rectilinear forms. As demonstrated by the reassembled West wall, approximately the same amount of material arranged in a planar lattice structure can effectively resist both gravity and lateral loads, thus sheathing would not be required for structural performance, potentially leading to flexibility in how such a wall unit would be designed in the future. With the growing availability of flexible robotic fabrication setups these results challenge the traditional notion that timber framing must adhere to rectilinear forms, which have been developed for ease of manual construction.

6 Conclusion

This paper presented the computational workflow used for planning cooperative robotic disassembly and reassembly tasks on an existing timber structures, which builds on our preliminary work-in-progress conference publication on the same topic (Bruun et al. 2022b) The current paper demonstrated how cooperative robotic setup could be used to collect as-built geometric data on an unknown structure, while also being used to physically execute planned fabrication tasks involving placing/removing elements while simultaneously supporting the structure. The ZeroWaste project demonstrated how considerations for material reduction and reuse can be paired with the capabilities of contemporary cooperative robotic fabrication setups.

6.1 Summary of results

The paper started by introducing the computational methods developed for the ZeroWaste project. These methods were subsequently applied to achieve research objectives related to circular economy principles and the use of robotic fabrication methods.

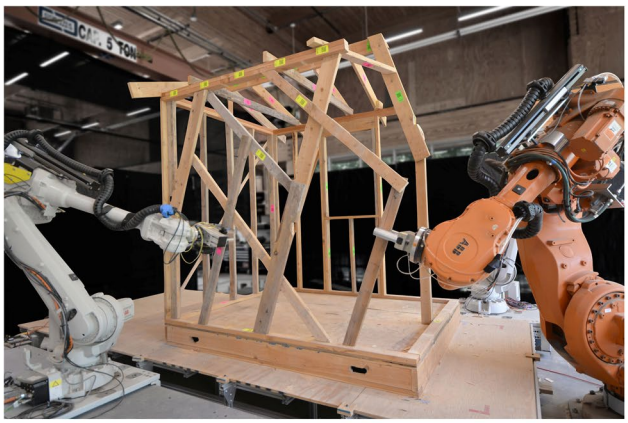

(a) Step 24 in the disassembly/reassembly sequence showing R2 placing the final member into the planar wall (from blinded).

(b) Elevation of the finished West wall reassembled into a lattice structure.

Fig. 22 The prototype structure at the end of the disassembly and reassembly in Phase 3

In terms of circular economy objectives, we successfully executed three fabrication case studies on the prototype structure that demonstrated the potential for existing timber buildings to function as reservoirs for reusable materials. By executing varying degrees of disassembly and reassembly on an unidentified timber prototype structure, we showed how new structural configurations could be created from previously utilized materials. We demonstrated the "narrow" circular economy principle, by avoiding the need to use any external temporary supporting scaffolding during fabrication. We demonstrated the "slow" circular economy principle, through the reuse of existing material.

In terms of computational and cooperative robotic fabrication methods, the project utilized a robotic cell equipped with three large-scale robotic arms. Initially, 3D cameras mounted on the robots captured precise geometric data of the prototype structure, aiding in efficient robotic sequence planning. Subsequently, a novel graph-based representation known as the support hierarchy graph was developed to depict the order of member support in the structure, facilitating the calculation of structurally stable fabrication sequences through algorithmic operations. These sequences were further assessed for feasibility considering factors such as robotic reach and structural stability. Leveraging the cooperative potential of the robotic setup, the planned fabrication sequences were executed, with the robots simultaneously removing/placing members while providing temporary structural support as needed for stability. This approach enabled the execution of fabrication sequences without external temporary scaffolding, as the robots served as passive structural support.

Across three distinct phases of physical case studies on the prototype structure, the ZeroWaste project highlighted the potential of reducing reliance on scaffolding and virgin resources during construction. Phase 1 centered on the removal of a single targeted member, validating the computational and cooperative robotic workflow, and demonstrating scaffold-free cooperative robotic disassembly through a sequence executed by two robots. Phase 2 expanded the disassembly objective to encompass a larger portion of the structure-the full South wall-utilizing all three available robots and incorporating structural reassembly to highlight the potential for reusing extracted members. Phase 3 went further by disassembling all remaining members in the West wall and roof sub-structures, introducing stricter constraints in reassembly. Each extracted member was reincorporated to reshape the West wall into a new lattice configuration, thereby enhancing its lateral stiffness. Through the successful execution of these phases, the ZeroWaste project illustrated the feasibility of orchestrating scaffold-free cooperative robotic disassembly and reassembly processes for existing timber structures, setting the stage for more sustainable construction practices.

6.2 Limitations and future work

While the current study has made significant contributions in developing and demonstrating methods for advancing scaffold-free cooperative robotic disassembly and reassembly processes for existing timber structures, several limitations and avenues for future research remain to be addressed to improve the scalability and the broader applicability of this research.

Real-time Feedback on As-built Geometry: An inherent limitation of our current approach lies in the reliance on pre-scanning the structure to generate a point cloud before beginning the planning of a particular fabrication phase. The method developed lacks the ability update the point cloud model promptly and accurately with changes during fabrication, necessitating a complete re-scan of the structure for any major changes to be updated in the model. Future research should prioritize the development of processes enabling the robots to dynamically collect information and update the as-built point cloud model of the structure while concurrently performing fabrication tasks. Such a real-time feedback mechanism would improve adaptability and accuracy in planning and executing fabrication processes, particularly for geometrically complex and dynamically changing structures.

Automating Point Cloud Processing for Feasibility Assessments: Another area requiring attention is the reduction of manual steps involved in setting up and processing the results of the path-planning and reachability feasibility assessments. Currently, users must manually select several locations on the point cloud representation of a member selected in a sequence only to conduct a series of brute force path-planning and reachability checks at these locations, a process that is both time-consuming and labor-intensive. Future research avenues would be to explore automated methods to streamline this process, potentially leveraging machine learning algorithms and computer vision techniques to automate point cloud processing with respect to performing these path-planning checks. Similarly, the implementation of a more automated approach to creating the finite element model based on the as-built point cloud holds promise for significant reductions in time required for the structural feasibility assessments. Currently, users are tasked with processing the point cloud manually to construct the structural analysis model for each sequence, based on the centerline locations of members.

Integrating Results of Finite Element Analysis with Graph Representation: Enhanced integration between finite element analysis results and the support hierarchy graph representation could optimize the generation and selection of fabrication sequences. Currently, all graph edges have uniform weights, but updating them dynamically based on previous analysis findings would facilitate a more informed sequence generation process. For example, this could take the form of updating edge weights based on the structural loading the members experienced in a previous step. But other user-specified criteria could also be set. Overall, better linking integration of the finite element analysis and the graph representation would help reduce the extensive set of potential sequences currently generated and then verified.

Use of Mobile Robots: The inclusion of mobile robots for specific tasks, such as data gathering and material handling, holds promise for enhancing the overall scalability and broader applicability of the methods developed in this project. Utilizing mobile robots alongside stationary robotic arms would enable a better distribution of labor between the robots and broaden the overall reach of the cooperative setup allowing it to manage more diverse construction scenarios. It would also allow for larger structures to be disassembled, as currently the physical limit is set by the fixed volume of the robotic setup. In addition, fasteners are currently removed manually, and a mobile robot could instead be used to perform this function.

Life-Cycle Analysis: Analyzing the environmental impact of using robots to replace traditional methods on a job site would provide a clearer understanding of the pros and cons of different approaches. While our research primarily focused on showcasing cooperative robotic scaffold-free

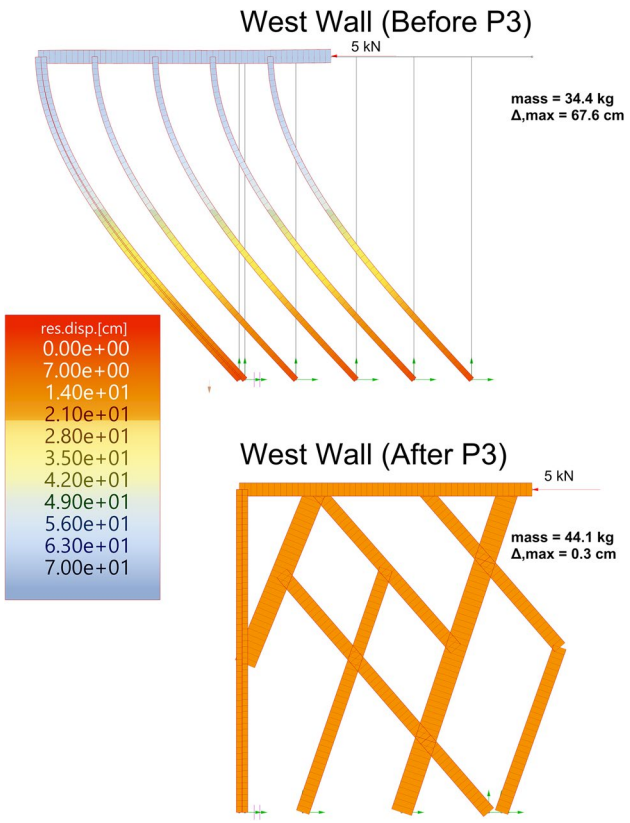

Fig. 23 Finite element analysis comparing the lateral stiffness of the original (top) to the reassembled (bottom) West wall

disassembly and reassembly processes, performing an energy balance or life-cycle analysis of these processes in the future is essential to determine the true impact of robot utilization.

In conclusion, addressing these limitations and pursuing future research directions will further advance the capabilities of cooperative robotic fabrication systems in the construction industry, to target the lack of efficiency in the construction section as a whole, and contribute to more sustainable construction practices.

Appendix A: Code for topological support hierarchy

A.1. Breadth-first search subgraph calculation functions

Calculate subgraphs for individual user-specified active members

```
function CALC_SUBG(G, rm_memb)
    nodes_queue ← [rm_memb]
    nodes_checked ← []

    while nodes_queue is not empty do
        n_check ← nodes_queue.pop(0)
        node_type ← _check_node_type(G, n_check, rm_memb)
        if node_type in ["remove","normal","normal_1side_fixed"] then
            nodes_queue, nodes_checked ← _find_adjacent_nodes(G, n_check, nodes_queue,nodes_checked)
        end if
        nodes_checked.append(n_check)
        node_draw_settings(G, [n_check], node_type)
    end while

    return G.subgraph(odes_checked)
end function
```

```
function _CHECK_NODE_TYPE(G, n_check, rm_membs)
    in_degree ← G.in_degree(n_check)
    out_degree ← G.out_degree(n_check)
    fixed_sides_count ← _count_fixed_sides(G, n_check)

    if n_check in rm_membs and in_degree == 0 then
        node_type ← "remove_start"
    else if n_check in rm_membs then
        node_type ← "remove"
    else if in_degree == 0 then
        node_type ← "start"
    else if out_degree == 0 then
        node_type ← "end_foundation"
    else if fixed_sides_count == 2 then
        node_type ← "end_2sides_fixed"
    else if fixed_sides_count == 1 then
        if _check_if_fixed_exists_multi(G, n_check, rm_membs) then
            node_type ← "danger_1side_fixed"
        else if not any(G.has_edge(n_check, m) for m in rm_membs) then
            node_type ← "danger_1side_fixed"
        else
            node_type ← "normal_1side_fixed"
        end if
    else
        node_type ← "normal"
    end if

    return node_type
end function
```

A.2. Fixed member check functions

Check if any members with a fixed connection are fully removed

```
function FXD_NODES_CUT(G, K)
    fxd_n_cut_rmv ← set()
    for n in K.nodes() do
        fully_removed ← (K.in_degree(n) + K.out_degree(n)) == (G.in_degree(n) + G.out_degree(n))
        if fully_removed then
            in_edges, out_edges ← set(K.in_edges(n)), set(K.out_edges(n))
            fixed_edges ← in_edges.intersection([(v, u) for u, v in out_edges])
            if fixed_edges is not empty then
                fxd_n_cut_rmv.update(v for u, v ∈ fixed_edges)
            end if
        end if
    end for
    return list(fxd_n_cut_rmv)
end function
```

A.3. Disassembly sequence functions

Check support conditions of any fixed members in a subgraph

```
function FXD_NODES_SUPPORT(G, K, rm_membs, fxd_n_cut_rmv)
    fxd_n_check ← []
    for n_check in K.nodes() do
        node_type ← _check_node_type(G,n_check,rm_membs)
        if node_type in ["end_2sides_fixed","danger_1side_fixed"] then
            fxd_n_check.append(n_check)
        end if
    end for
    n_safe_fix1, n_safe_fix2, n_notsafe ← _check_connected(G, K, fxd_n_cut_rmv, fxd_n_check)
end function
```

```
function _CHECK_CONNECTED(G, K, fxd_n_cut_rmv,fxd_n_check)
    n_safe_fix1,n_safe_fix1,n_notsafe ← [],[],[]
    for n in fxd_n_check do
        e_G,e_K ← list(G.out_edges(n)),list(K.out_edges(n))
        num_supports, flag ← (len(e_G) - len(e_K)), False
        for (u,v) in e_K do
            if _check_if_fixed_exists(G, u, v) then
                if u ∉ fxd_n_cut_rmv and v ∉ fxd_n_cut_rmv then
                    num_supports,flag ← num_supports+1, True
                end if
            end if
        end for
        if num_supports < 2 then
            n_notsafe.append(n)
        else if _count_fixed_sides(G, n) == 2 and flag then
            n_safe_fix2.append(n)
        else if _count_fixed_sides(G, n) == 2 then
            n_safe_fix1.append(n)
        else if _count_fixed_sides(G, n) == 1 then
            n_safe_fix1.append(n)
        end if
    end for
    return n_safe_fix1,n_safe_fix2,n_notsafe
end function
```

Select any members for a free robot to grip as support

```
function SET_N_TO_ROB_SUPPORT(K)
    select ← yes/no
    if select then
        n ← selected members that will be supported in the next step
        node_draw_settings(K, n, "rob_sprt")
    end if
end function
```

Find and select active members in the current subgraph for this step of the sequence

```
function FIND_N_ACTIVE(K, n_type)
    if any n_type in K.nodes() then
        n_active ← n_type in K.nodes()
    else
        n_active ← []
    end if
    return n_active
end function
```

```
function SELECT_N_ACTIVE(n1,n2)
    n_rob_sprt ← n2
    number_of_free_robs ← number_of_total_robs - number_of_robs_supporting
    for rob in number_of_free_robs do
        n_rmv ← choose n in n1 to remove
        n_rob_sprt ← choose additional n in n1 to support
    end for
    node_draw_settings(K, n_rmv, "start")
    node_draw_settings(K, n_rob_sprt, "rob_sprt")
    return n_rmv,n_rob_sprt
end function
```

Relabel subgraph with new potential start nodes after the current step is executed

```
function NEW_SUBG_RELABEL(K, rms)
    K_new ← _relabel_from_connectivity(K,rms)
    K_new ← _relabel_from_rob_support(K_new)
    K_new ← _relabel_from_fixed_supports(K_new)
    K_new ← _relabel_from_end_conditions(K_new)
    return K_new
end function
```

Appendix B: Fabrication photos

B.1. Phase 1

See Fig. 24.

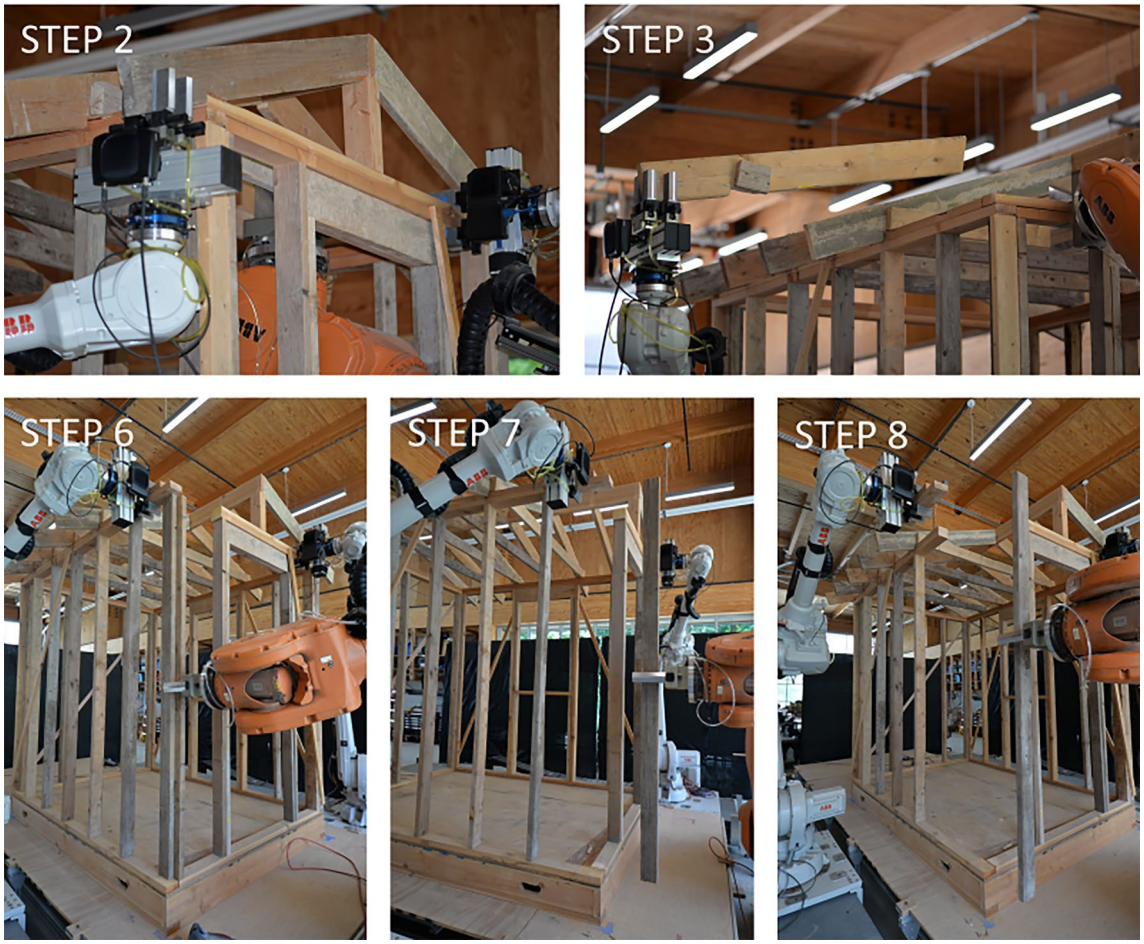

Fig. 24 Phase 1 fabrication photos

B.2. Phase 2

See Figs. 25, 26.

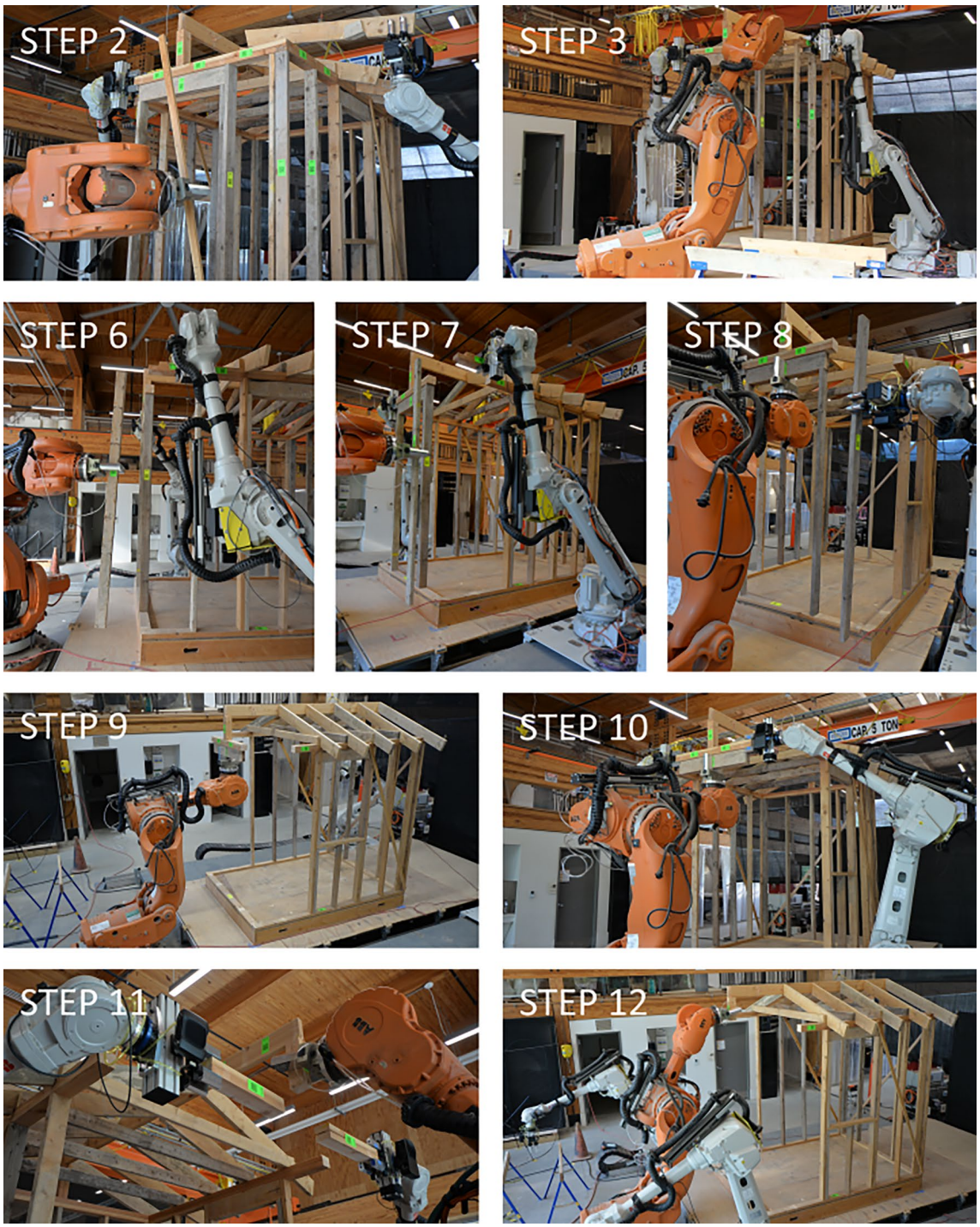

Fig. 25 Phase 2 fabrication photos (disassembly)

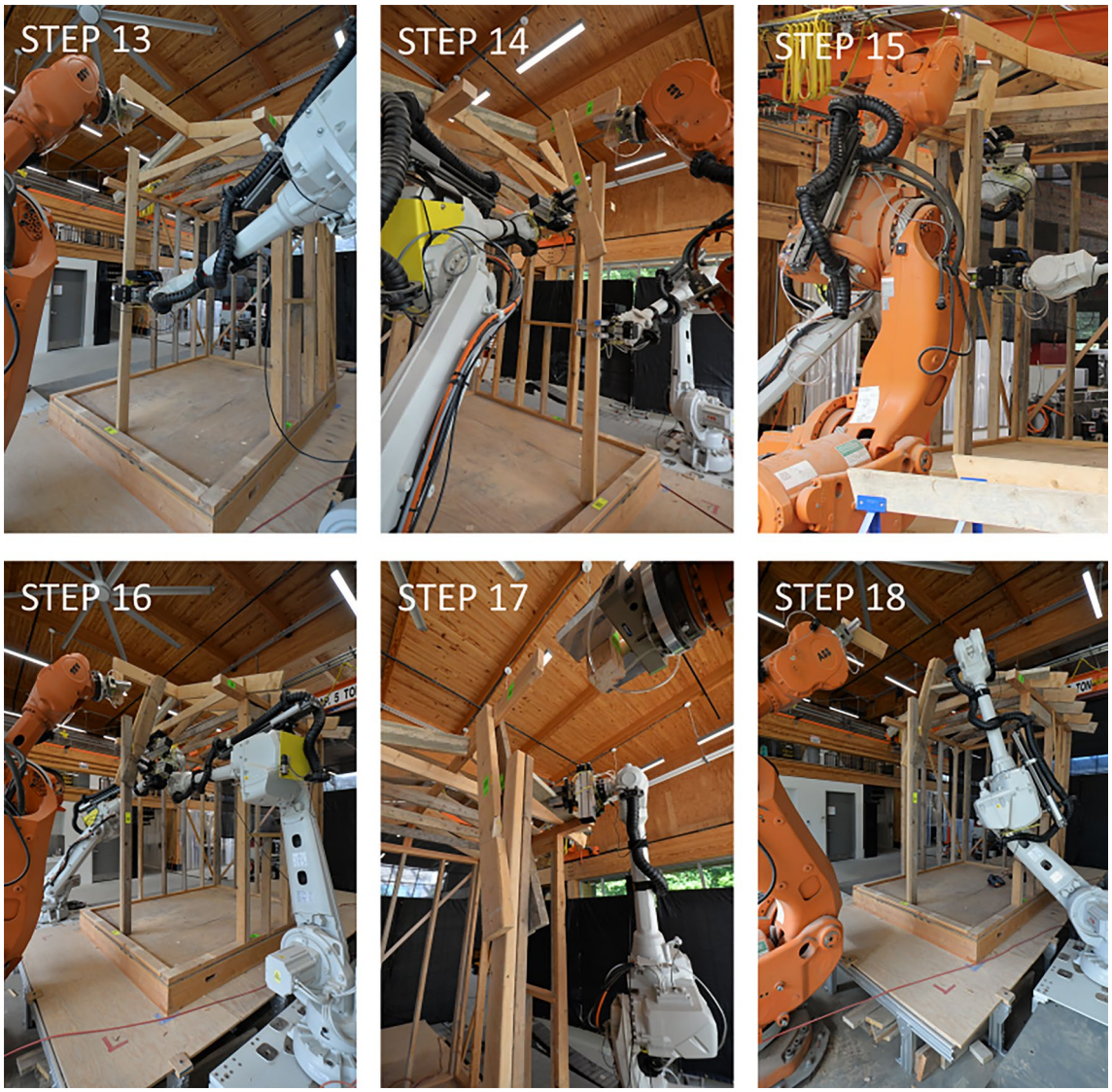

Fig. 26 Phase 2 fabrication photos (reassembly)

B.3. Phase 3

See Figs. 27, 28, 29

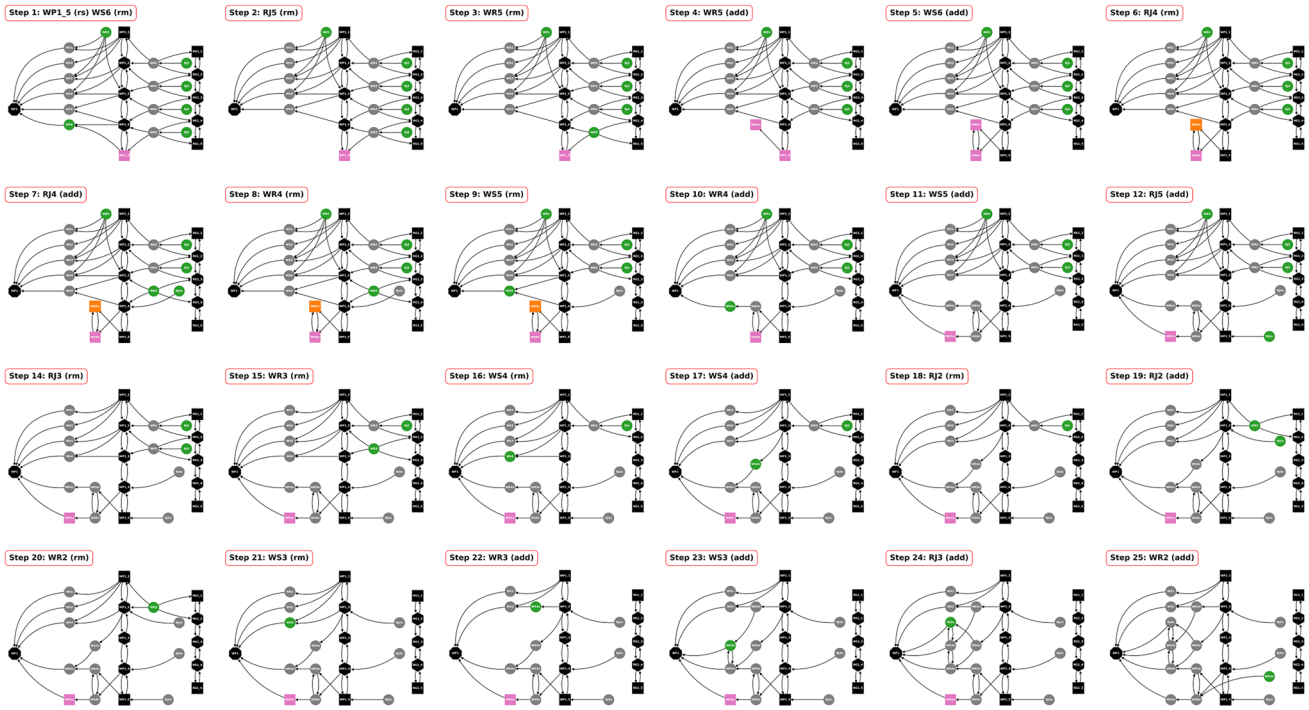

Fig. 27 Phase 3 subgraphs corresponding to steps in sequence

Fig. 28 Phase 3 first half of disassembly/reassembly photos

Fig. 29 Phase 3s half of disassembly/reassembly photos

Supplementary Information The online version contains supplementary material available at https://doi.org/10.1007/s41693-024-00137-7.

Acknowledgements We would like to thank the following people for their help at various stages throughout the project: Chris Myefski, Chase Galis, Ian Ting, John Mikesh. In addition, we would like to acknowledge the industry support from Zivid, in the form of reduced pricing for their high-end 3D color camera. The project is funded in part by National Science Foundation (Grant No. 2122271) and Princeton University (Campus as a Lab Fund).

Data availability Data is available upon request.

Declarations

Conflict of interest On behalf of all authors, the corresponding author states that there is no Conflict of interest.

References

American Wood Council (2015) National Design Specification for wood construction with commentary. 2015 edition ed., American Wood Council, Leesburg, VA. ISBN: 978-1-940383-38-5

Amtsberg F, Yang X, Skoury L, Wagner HJ, Menges A (2021) iHRC: An AR-based interface for intuitive, interactive and coordinated task sharing between humans and robots in building construction, In: Proceedings of the 38th International Symposium on Automation and Robotics in Construction (ISARC), International Association for Automation and Robotics in Construction (IAARC), Dubai, UAE. pp. 25–32. https://doi.org/10.22260/ISARC2021/0006

Barbosa F, Woetzel J, Mischke J, Ribeirinho M, Sridhar M, Parsons M, Bertram N, Brown S (2017) Reinventing Construction: A Route to Higher Productivity. Technical Report. McKinsey Global Institute. https://www.mckinsey.com/business-functions/operations/our-insights/reinventing-construction-through-a-productivity-revolution

Bock T (2007) Construction robotics. Auton Robots 22:201–209. https://doi.org/10.1007/s10514-006-9008-5

Bock T, Linner T (2016) Construction robots: elementary technologies and single-task construction robots, vol 4. Cambridge University Press, Cambridge

Bocken NMP, de Pauw I, Bakker C, van der Grinten B (2016) Product design and business model strategies for a circular economy. J Ind Prod Eng 33:308–320. https://doi.org/10.1080/21681015.2016.1172124

Bonwetsch T, Gramazio F, Kohler M (2007) Digitally fabricating non-standardised brick walls, In: ManuBuild, pp 191–196. ISBN: 978-0-86017-710-4

Bonwetsch T, Kobel D, Gramazio F, Kohler M (2006) The informed wall: applying additive digital fabrication techniques on architecture, In: Proceedings of the 25th annual conference of the association for computer-aided design in architecture, pp 489–495. ISBN: 978-0-9789463-0-2

Bruun EPG, Adriaenssens S, Parascho S (2022a) Structural rigidity theory applied to the scaffold-free (dis)assembly of space frames using cooperative robotics. Autom Constr 141:104405. https://doi.org/10.1016/j.autcon.2022.104405

Bruun EPG, Adriaenssens S, Besler E, Parascho S (2022b) ZeroWaste: towards computing cooperative robotic sequences for the disassembly and reuse of timber frame structures. Proceedings of the 42nd annual conference of the association for computer aided design in architecture, pp 586–597. http://arks.princeton.edu/ark:/88435/pr1wp9t657

Bruun EPG, Parascho S, Adriaenssens S (2024) Cooperative robotic fabrication for a circular economy, In: De Wolf C, Çetin S, Bocken N (eds) A circular built environment in the digital age. Springer Cham. Circular Economy and Sustainability, pp 129–149. https://doi.org/10.1007/978-3-031-39675-5_8

Bruun EPG, Pastrana R, Paris V, Beghini A, Pizzigoni A, Parascho S, Adriaenssens S (2021) Three cooperative robotic fabrication methods for the scaffold-free construction of a masonry arch. Autom Constr 129:103803. https://doi.org/10.1016/j.autcon.2021.103803

Bruun EPG, Ting I, Adriaenssens S, Parascho S (2020) Human-robot collaboration: a fabrication framework for the sequential design and construction of unplanned spatial structures. Digit Creat 31:320–336. https://doi.org/10.1080/14626268.2020.1845214

Brütting J, Desruelle J, Senatore G, Fivet C (2019) Design of truss structures through reuse. Structures 18:128–137. https://doi.org/10.1016/j.istruc.2018.11.006

Brütting J, Senatore G, Fivet C (2021) Design and fabrication of a reusable kit of parts for diverse structures. Autom Constr 125:103614. https://doi.org/10.1016/j.autcon.2021.103614

Brütting J, Senatore G, Schevenels M, Fivet C (2020) Optimum design of frame structures from a stock of reclaimed elements. Front Built Environ 6:57. https://doi.org/10.3389/fbuil.2020.00057

Bärtschi R, Knauss M, Bonwetsch T, Gramazio F, Kohler M (2010) Wiggled brick bond. Advances in architectural geometry 2010. Springer, Wien/New York, pp 137–147. https://doi.org/10.1007/978-3-7091-0309-8

Cao YU, Fukunaga AS, Kahng A (1997) Cooperative mobile robotics: antecedents and directions. Auton Robots 4:7–27. https://doi.org/10.1023/A:1008855018923

Cottafava D, Ritzen M (2021) Circularity indicator for residential buildings: Addressing the gap between embodied impacts and design aspects. Resour Conserv Recycl. https://doi.org/10.1016/j.resconrec.2020.105120

De Wolf C, Çetin S, Bocken N (2023) A circular built environment in the digital age. Circular economy and sustainability. Springer, Cham. https://doi.org/10.1007/978-3-031-39675-5

Diyamandoglu V, Fortuna LM (2015) Deconstruction of wood-framed houses: material recovery and environmental impact. Resour Conserv Recycl 100:21–30. https://doi.org/10.1016/j.resconrec.2015.04.006

Doerstelmann M, Knippers J, Menges A, Parascho S, Prado M, Schwinn T (2015) ICD/ITKE research pavilion 2013–2014: modular coreless filament winding based on beetle elytra. Arch Des 85:54–59. https://doi.org/10.1002/ad.1954

Dörfler K, Sandy T, Giftthaler M, Gramazio F, Kohler M, Buchli J (2016) Mobile robotic brickwork: automation of a discrete robotic fabrication process using an autonomous mobile robot, In: Robotic fabrication in architecture, art and design 2016, Springer International Publishing, Sydney, Australia. pp 204–217. https://doi.org/10.1007/978-3-319-26378-6-15

Eberhardt L, Rønholt J, Birkved M, Birgisdottir H (2021) Circular Economy potential within the building stock—mapping the embodied greenhouse gas emissions of four Danish examples. J Build Eng 33:101845. https://doi.org/10.1016/j.jobe.2020.101845

Fang D, Brown N, De Wolf C, Mueller C (2023) Reducing embodied carbon in structural systems: a review of early-stage design strategies. J Build Eng 76:107054. https://doi.org/10.1016/j.jobe.2023.107054

Fishbein BK (1998) Building for the future: strategies to reduce construction and demolition waste in municipal projects. volume 5 of INFORM Special Report. INFORM, Inc., New York

Fleischmann P, Casas G, Lyrenmann M (2020) COMPAS RRC: Online control for ABB robots over a simple-to-use Python interface. https://doi.org/10.5281/zenodo.4639418

Garcia AB, Cebeci IY, Calvo RV, Gordon M (2021) Material (data) intelligence - towards a circular building environment, In: Proceedings of the 26th international conference of the association for computer-aided architectural design research in Asia, pp 361–370. https://doi.org/10.52842/conf.caadria.2021.1.361

Geissdoerfer M, Savaget P, Bocken NMP, Hultink EJ (2017) The circular economy—a new sustainability paradigm? J Clean Prod 143:757–768. https://doi.org/10.1016/j.jclepro.2016.12.048

Giftthaler M, Sandy T, Dörfler K, Brooks I, Buckingham M, Rey G, Kohler M, Gramazio F, Buchli J (2017) Mobile robotic fabrication at 1:1 scale: the in situ fabricator. Constr Robot 1:3–14. https://doi.org/10.1007/s41693-017-0003-5

Glath J, Gobin T, Mesnil R, Mimram M, Baverel O (2022) Thinking and designing reversible structures with non-sequential assemblies. Design modeling symposium: towards radical regeneration. Springer International Publishing, Berlin, pp 249–259. https://doi.org/10.1007/978-3-031-13249-0_21

Gramazio F, Kohler M (2008) Digital materiality in architecture, 1st edn. Lars Muller, Baden

Gramazio F, Kohler M (eds) (2014) Made by robots: challenging architecture at a larger scale, 1st edn. Academy Press, London

Hack N, Dörfler K, Walzer AN, Wangler T, Mata-Falcón J, Kumar N, Buchli J, Kaufmann W, Flatt RJ, Gramazio F, Kohler M (2020) Structural stay-in-place formwork for robotic in situ fabrication of non-standard concrete structures: a real scale architectural

demonstrator. Autom Constr 115:1–13. https://doi.org/10.1016/j.autcon.2020.103197
Hack N, Wangler T, Mata-Falcón J, Dörfler K, Kumar N, Walzer N, Graser K, Reiter L, Richner H, Buchli J, Kaufmann W, Flatt RJ, Gramazio F, Kohler M (2017) Mesh mould: an on site, robotically fabricated, functional formwork, In: Second concrete innovation conference, Tromsø, Norway. p 11. ISBN: 978-82-8208-054-5
Hagberg AA, Schult DA, Swart PJ (2008) Exploring network structure, dynamics, and function using NetworkX, In: Proceedings of the 7th Python in science conference, Pasadena, CA USA. pp 11–15. http://conference.scipy.org.s3-website-us-east-1.amazonaws.com/proceedings/scipy2008/index.html
Han IX, Bruun EPG, Marsh S, Adriaenssens S, Parascho S (2020) From concept to construction: a transferable design and robotic fabrication method for a building-scale vault, In: Proceedings of the 40th annual conference of the association for computer aided design in architecture, Online. pp 614–623. https://doi.org/10.52842/conf.acadia.2020.1.614
International Energy Agency, United Nations Environment Programme (2018) 2018 Global status report: Towards a zero-emission, efficient and resilient buildings and construction sector. Technical Report. Global Alliance for Buildings and Construction. https://wedocs.unep.org/20.500.11822/27140
Kaethner S, Burridge J (2012) Embodied CO2 of structural frames. Struct Eng 90:33–40
Kohler M, Gramazio F, Willmann J (2014) Gantenbein vineyard façade. The robotic touch: how robots change architecture. The University of Chicago Press, Chicago, pp 66–75
Konietzko J, Bocken N, Hultink E (2020) Circular ecosystem innovation: an initial set of principles. J Clean Prod 253:119942. https://doi.org/10.1016/j.jclepro.2019.119942
Lu W, Yuan H (2011) A framework for understanding waste management studies in construction. Waste Manage (Oxf) 31:1252–1260. https://doi.org/10.1016/j.wasman.2011.01.018
Mele TV et al., (2017) COMPAS: a framework for computational research in architecture and structures. https://doi.org/10.5281/zenodo.2594510
Mesnil R, Gobin T, Demont L, Margerit P, Ducoulombier N, Douthe C, Caron JF (2023) Flexible digital manufacturing of timber construction: the design and fabrication of a free-form nexorade. Constr Robot 7:193–212. https://doi.org/10.1007/s41693-023-00105-7
Mills TH, Showalter E, Jarman D (1999) A cost-effective waste management plan. Cost Eng 41:35–43
Naboni R, Kunic A, Kramberger A, Schlette C (2021) Design, simulation and robotic assembly of reversible timber structures. Constr Robot 5:13–22. https://doi.org/10.1007/s41693-020-00052-7
O'Brien E, Guy B, Lindner AS (2006) Life cycle analysis of the deconstruction of military barracks: Ft. McClellan, Anniston AL. J Green Build 1:166–183. https://doi.org/10.3992/jgb.1.4.166
Osmani M, Glass J, Price A (2008) Architects' perspectives on construction waste reduction by design. Waste Manage (Oxf) 28:1147–1158. https://doi.org/10.1016/j.wasman.2007.05.011
Parascho S (2023) Construction robotics: from automation to collaboration. Annu Rev Control Robot Auton Syst. https://doi.org/10.1146/annurev-control-080122-090049
Parascho S, Gandia A, Mirjan A, Gramazio F, Kohler M (2017) Cooperative fabrication of spatial metal structures. Fabricate 2017: rethinking design and construction. UCL Press, London, pp 24–29. https://doi.org/10.3929/ethz-b-000219566
Parascho S, Han IX, Beghini A, Miki M, Walker S, Bruun EPG, Adriaenssens S (2021) LightVault: a design and robotic fabrication method for complex masonry structures, In: Advances in architectural geometry 2020, Presses des Ponts, Paris, France. pp 350–375. https://oar.princeton.edu/handle/88435/pr1s17ss4d
Parascho S, Han IX, Walker S, Beghini A, Bruun EPG, Adriaenssens S (2020) Robotic vault: a cooperative robotic assembly method for brick vault construction. Constr Robot 4:117–126. https://doi.org/10.1007/s41693-020-00041-w
Parascho S, Kohlhammer T, Coros S, Gramazio F, Kohler M (2018) Computational design of robotically assembled spatial structures: a sequence based method for the generation and evaluation of structures fabricated with cooperating robots, In: Advances in architectural geometry 2018, Klein Publishing GmbH, Gothenburg, Sweden. pp 112–139. https://research.chalmers.se/en/publication/504188
Piškorec L, Jenny D, Parascho S, Mayer H, Gramazio F, Kohler M (2018) The brick labyrinth, In: Robotic fabrication in architecture, art and design 2018, Springer International Publishing, Zurich. pp. 489–500. https://doi.org/10.1007/978-3-319-92294-2_37
Preisinger C, Heimrath M (2014) Karamba-a toolkit for parametric structural design. Struct Eng Int 24:217–221. https://doi.org/10.2749/101686614X13830790993483
Purchase CK, Zulayq DMA, O'Brien BT, Kowalewski MJ, Berenjian A, Tarighaleslami AH, Seifan M (2022) Circular economy of construction and demolition waste: a literature review on lessons, challenges, and benefits. Materials. https://doi.org/10.3390/ma15010076
Ritchie H, Samborska V, Roser M (2024) Urbanization. https://ourworldindata.org/urbanization
Rust R, Casas G, Parascho S, Jenny D, Dörfler K, Helmreich M, Gandia A, Ma Z, Ariza I, Pacher M, Lytle B, Huang Y, Kasirer C, Bruun E (2018) COMPAS FAB: robotic fabrication package for the COMPAS framework. https://doi.org/10.5281/zenodo.3469478
Rutten D (2007) Grasshopper. https://www.grasshopper3d.com/
Shi J, Jimmerson G, Pearson T, Menassa R (2012) Levels of human and robot collaboration for automotive manufacturing, In: Proceedings of the workshop on performance metrics for intelligent systems, ACM, College Park Maryland. pp 95–100. https://doi.org/10.1145/2393091.2393111
García de Soto B, Agustí-Juan I, Hunhevicz J, Joss S, Graser K, Habert G, Adey BT (2018) Productivity of digital fabrication in construction: cost and time analysis of a robotically built wall. Autom Constr 92:297–311. https://doi.org/10.1016/j.autcon.2018.04.004
Søndergaard A, Feringa J, Nørbjerg T, Steenstrup K, Brander D, Graversen J, Markvorsen S, Bærentzen A, Petkov K, Hattel J, Clausen K, Jensen K, Knudsen L, Kortbek J (2016) Robotic hot-blade cutting, In: Robotic fabrication in architecture, art and design 2016, Springer International Publishing, Sydney, Australia. pp 150–164. https://doi.org/10.1007/978-3-319-26378-6_11
The Business Research Company (2023) Global construction market report and strategies 2022. Technical Report. The Business Research Company. https://www.thebusinessresearchcompany.com/report/construction-market
Thoma A, Adel A, Helmreich M, Wehrle T, Gramazio F, Kohler M (2018) Robotic fabrication of bespoke timber frame modules. Robotic fabrication in architecture, art and design 2018. Springer International Publishing, Zurich, pp 447–458. https://doi.org/10.1007/978-3-319-92294-2_34
United Nations (2021) Global Status Report for Buildings and Construction. Technical Report. UN. https://globalabc.org/sites/default/files/2021-10/GABC_Buildings-GSR-2021_BOOK.pdf
US EPA (1998) Characterization of building-related construction and demolition debris in the United States. Technical Report EPA530-R-98-010. Municipal and Industrial Solid Waste Division. https://archive.epa.gov/epawaste/hazard/generation/web/pdf/cd-rpt.pdf
US EPA (2018) Construction and demolition debris generation in the United States, 2015. Technical Report. Office of Resource Conservation and Recovery. https://www.epa.gov/facts-and-figures-about-materials-waste-and-recycling/studies-summary-tables-and-data-related
US EPA (2020a) Advancing sustainable materials management: 2018 Fact Sheet. Technical Report. Office of Resource Conservation

and Recovery. https://www.epa.gov/sites/default/files/2021-01/documents/2018_ff_fact_sheet_dec_2020_fnl_508.pdf
US EPA (2020b) Construction and demolition debris management in the United States, 2015. Technical Report. Office of Resource Conservation and Recovery. https://www.epa.gov/sites/production/files/2020-03/documents/final_cd-eol-management_2015_508.pdf
Valiente G (2021) Algorithms on trees and graphs: with Python code, 2nd edn. Springer, Cham
Weckenborg C, Kieckhäfer K, Müller C, Grunewald M, Spengler TS (2020) Balancing of assembly lines with collaborative robots. Bus Res 13:93–132. https://doi.org/10.1007/s40685-019-0101-y
Willmann J, Knauss M, Bonwetsch T, Apolinarska AA, Gramazio F, Kohler M (2016) Robotic timber construction—expanding additive fabrication to new dimensions. Autom Constr 61:16–23. https://doi.org/10.1016/j.autcon.2015.09.011
Wu K, Kilian A (2018) Robotic equilibrium: Scaffold free arch assemblies, In: Proceedings of the 38th annual conference of the association for computer aided design in architecture, Mexico City. pp 342–349. https://doi.org/10.52842/conf.acadia.2018.342
Yang X, Amtsberg F, Sedlmair M, Menges A (2024) Challenges and potential for human-robot collaboration in timber prefabrication. Autom Constr 160:105333. https://doi.org/10.1016/j.autcon.2024.105333
Zahiri N (2023) Sequential augmented assembly of interlocking timber elements for circular wood construction, In: Proceedings of the IASS Annual Symposium 2023, International association for shell and spatial structures, Melbourne. p 12. https://www.ingentaconnect.com/contentone/iass/piass/2023/00002023/00000018/art00010
Zhou QY, Park J, Koltun V (2018) Open3D: A Modern Library for 3D Data Processing. arXiv https://doi.org/10.48550/arXiv.1801.09847
Zimmann R, O'Brien H, Hargrave J, Morrell M (2016) The circular economy in the built environment. Technical Report. Arup. https://www.arup.com/perspectives/publications/research/section/circular-economy-in-the-built-environment
Zivid AS (2021) Zivid Two. Technical Specifications. Zivid AS. Oslo, Norway. https://www.zivid.com/zivid-2-specs
Çetin S, De Wolf C, Bocken N (2021) Circular digital built environment: an emerging framework. Sustainability 13:6348. https://doi.org/10.3390/su13116348